Resilient Trajectory Tracking to Partial Loss of Control Authority over Actuators with Actuation Delay

Jean-Baptiste Bouvier*   Himmat Panag*   Robyn Woollands*

Melkior Ornik*

March 24, 2023

Abstract

After the loss of control authority over thrusters of the Nauka module, the International Space Station lost attitude control for 45 minutes with potentially disastrous consequences. Motivated by a scenario of orbital inspection, we consider a similar malfunction occurring to the inspector satellite and investigate whether its mission can still be safely fulfilled. While a natural approach is to counteract in real-time the uncontrolled and undesirable thrust with the remaining controlled thrusters, vehicles are often subject to actuation delays hindering this approach. Instead, we extend resilience theory to systems suffering from actuation delay and build a resilient trajectory tracking controller with stability guarantees relying on a state predictor. We demonstrate that this controller can track accurately the reference trajectory of the inspection mission despite the actuation delay and the loss of control authority over one of the thrusters.

Notation

For a set $\mathcal{X} \subseteq \mathbb{R}^n$, $\dim(\mathcal{X})$ denotes its dimension, $\partial \mathcal{X}$ its boundary, $\text{co}(\mathcal{X})$ its convex hull, $\text{int}(\mathcal{X})$ its interior, and $\text{relint}(\mathcal{X})$ its relative interior as defined in [1]. The Minkowski addition of $\mathcal{X}$ and $\mathcal{Y} \subseteq \mathbb{R}^n$ is denoted by $\mathcal{X} \oplus \mathcal{Y} := \{x + y : (x, y) \in \mathcal{X} \times \mathcal{Y}\}$ and their Minkowski difference is $\mathcal{X} \ominus \mathcal{Y} := \{z \in \mathbb{R}^n : z + y \in \mathcal{X} \text{ for all } y \in \mathcal{Y}\}$. The set of all functions $f : [0, +\infty) \to \mathcal{X}$ is denoted by $\mathcal{F}(\mathcal{X})$. The closed ball of dimension b, radius $r \geq 0$, and center c is denoted $\mathbb{B}^b(c, r) := \{x \in \mathbb{R}^b : \|x - c\| \leq r\}$. For a set $\Lambda \subseteq \mathbb{C}$, we say that $Re(\Lambda) \leq 0$ (resp. $Re(\Lambda) = 0$) if the real part of each $\lambda \in \Lambda$ verifies $Re(\lambda) \leq 0$ (resp. $Re(\lambda) = 0$). The norm of a matrix A is $\|A\| := \sup_{x \neq 0} \frac{\|Ax\|}{\|x\|} = \max_{\|x\|=1} \|Ax\|$ and the set of its eigenvalues is $\Lambda(A)$. If A is positive definite, $A \succ 0$, then we define $\lambda_{min}^A := \min\{\Lambda(A)\}$, $\lambda_{max}^A := \max\{\Lambda(A)\}$ and the associated norm $\|x\|_A := \sqrt{x^\top A x}$. The controllability matrix of pair (A, B) is $\mathcal{C}(A, B) = \begin{bmatrix} B \, AB \, \ldots \, A^{n-1}B \end{bmatrix}$. The linear span of set $\mathcal{X}$ is denoted by $\text{span}(\mathcal{X}) := \{\sum_{i=1}^k \alpha_i x_i, \ k \in \mathbb{N}, \ \alpha_i \in \mathbb{R}, \ x_i \in \mathcal{X}\}$.

---

*Department of Aerospace Engineering and Coordinated Science Laboratory, University of Illinois at Urbana-Champaign, Urbana, IL 61801, USA. (bouvier3@illinois.edu).

1 Introduction

With an increase in the number of active satellites, there is a growing demand for on-orbit satellite inspection, e.g., to assess damage on satellites, prevent unnecessary spacewalks of astronauts, or enforce the ban of space weapons [2, 3, 4]. The importance of satellite inspection is also reflected by the creation of spacecraft entirely dedicated to on-orbit inspections, like the robot Laura from the Rogue Space Systems Corporation[1].

Partly inspired by the on-orbit servicing Restore-L mission [5], our scenario of interest consists of an *orbital inspection* of a satellite by a spacecraft that completes a full revolution around the target satellite. Following an on-board computer error, the inspecting spacecraft endures a *loss of control authority* [6] over one of its thrusters, similarly to what happened to the Nauka module when docked to the International Space Station [7]. This malfunction consists in one of the thrusters producing uncontrolled and thus possibly undesirable thrust with the same capabilities as before the malfunction.

Classically, changing or unknown dynamics are studied through robust, adaptive, and fault-tolerant control theories. However, robust control needs the undesirable thrust to be significantly smaller than the controlled thrust [8], which is not the case in our scenario. In turn, the estimators of adaptive controllers are unlikely to converge in the presence of uncontrolled thrust varying quickly [8]. Fault-tolerant theory provides a wider framework, but actuator failure investigations are usually limited either to completely disabled thrusters [9, 10], to actuators "locking in place" and producing constant inputs [11], or to actuators with reduced effectiveness [12, 13]. Since the uncontrolled thruster under study can still produce a full range of thrust, this malfunction is not covered by existing fault-tolerant theory [13]. Instead, we adopt the *resilience* framework [6, 14, 15] by assuming the presence of thrust sensors, thus enabling the implementation of fault-detection and isolation methods [16].

Because of the reaction times of the sensors and thrusters [16], the controller is likely not able counteract the undesirable thrust in real-time. Our objective is then to develop a control strategy for safely carrying out the inspection mission despite the malfunctioning thruster and the actuation delay. More specifically, we want the damaged spacecraft to accurately follow a safe reference trajectory. In our simulation, we choose a minimal-fuel reference trajectory generated by the convex optimization method of [17].

In the preliminary version of this work [18], resilience was not established analytically but empirically with a Monte-Carlo simulation. We address this issue by extending resilience theory to linear systems with actuation delay and by establishing a resilient trajectory tracking controller. Entirely new material includes Sections 3.2, 4, 5 and 6.

The main contributions of this work are fourfold. Firstly, we establish the resilience of a spacecraft with nonlinear dynamics. Secondly, we extend resilience theory to systems with actuation delay and provide sufficient conditions for these systems to be able to perform trajectory tracking. Thirdly, we build a resilient trajectory tracking controller with guaranteed performance for the nonlinear spacecraft dynamics. Finally, we demonstrate that on-orbit inspection can be performed safely despite actuation delay and a loss of control authority over a thruster.

The remainder of this paper is structured as follows. Section 2 introduces our problem of interest and the relative dynamics of the satellites. In Section 3, we ignore actuation delay to apply existing resilience theory to the malfunctioning spacecraft to demonstrate its remaining capabilities in terms of resilient reachability and trajectory tracking. Then, in Section 4 we

---

[1]https://rogue.space/orbots/

establish novel results to extend resilience theory to linear systems suffering from actuation delay. Section 5 builds on this theory to produce a resilient trajectory tracking controller with guaranteed performance despite actuation delay. Finally, Section 6 implements this controller in a numerical simulation of the inspection mission.

2   Motivation and background

We consider two spacecraft on circular orbit around Earth. The mission of the chaser spacecraft is to inspect the target spacecraft. As we are interested in proximity operations, we employ the Clohessy-Wiltshire equations in a local-vertical, local-horizontal frame [17]. The state vector $X = \begin{pmatrix} x & y & z & \dot{x} & \dot{y} & \dot{z} \end{pmatrix} \in \mathbb{R}^6$ represents the difference in position and velocity between the two spacecraft and initially follows the dynamics

$$\dot{X}(t) = AX(t) + r\bar{B}\bar{u}(t), \qquad X(0) = X_0 \in \mathbb{R}^6, \tag{1}$$

with a *thrust-to-mass ratio* $r = 1.5 \times 10^{-4}\,m/s^2$, as we consider a chaser spacecraft of mass $600\,kg$ and five PPS-1350 thrusters of maximal thrust $90\,mN$ [19] controlled by the inputs $\bar{u} = \begin{pmatrix} \bar{u}_1 & \bar{u}_2 & \bar{u}_3 & \bar{u}_4 & \bar{u}_5 \end{pmatrix} \in [0,1]^5$. Because the z-dynamics of the Clohessy-Witshire equations are decoupled from the other two axis, we focus on the two-dimensional dynamics in the (x,y)-plane, with matrices:

$$A = \begin{bmatrix} 0 & 0 & 1 & 0 \\ 0 & 0 & 0 & 1 \\ 3\Omega^2 & 0 & 0 & 2\Omega \\ 0 & 0 & -2\Omega & 0 \end{bmatrix} \qquad \text{and} \qquad \bar{B} = \begin{bmatrix} 0 & 0 & 0 & 0 & 0 \\ 0 & 0 & 0 & 0 & 0 \\ 1 & 1 & -1 & -\sqrt{2} & -1 \\ 1 & -1 & -1 & 0 & 1 \end{bmatrix},$$

where $\Omega = 0.00106\,s^{-1}$ is the mean orbital rate of the target's orbit. The thrusters do not create any torque [9] since they are rigidly fixed on the spacecraft and are aligned with its center of mass, as illustrated on Fig. 1. To perform its inspection mission, the chaser spacecraft relies on a fixed camera constantly pointing at the target thanks to the reaction wheels controlling the attitude of the chaser, as shown on Fig. 1. Because of these attitude changes, the relative dynamics lose their linearity to become

$$\dot{X}(t) = AX(t) + rR_\theta(t)\bar{B}\bar{u}(t), \qquad \text{with} \qquad R_\theta(t) = \begin{bmatrix} 1 & 0 & 0 & 0 \\ 0 & 1 & 0 & 0 \\ 0 & 0 & \cos\big(\theta(t)\big) & -\sin\big(\theta(t)\big) \\ 0 & 0 & \sin\big(\theta(t)\big) & \cos\big(\theta(t)\big) \end{bmatrix}, \tag{2}$$

where θ is illustrated on Fig. 1 and is defined as the 2-argument arctangent $\theta(t) := \operatorname{atan2}\big(y(t), x(t)\big)$.

Following the Restore-L protocol [5], we assume that the chaser must come within $80\,m$ of the target for a precise optical inspection. Hence, we want the chaser to occupy successively the 5 following holding points $(0, 80)$, $(-80, 0)$, $(0, -80)$, $(80, 0)$ and $(0, 80)$. Using the convex optimization method [17] we compute on Fig. 2 the minimal fuel trajectory linking these waypoints with 90 minutes transfers. For safety considerations, we consider a keep-out sphere (KOS) of radius $R_{KOS} = 50\,m$ around the target as in the Restore-L mission [5].

Because the chaser is constantly pointing its camera towards the target, its orientation angle θ (see Fig. 1) varies throughout the trajectory as shown on Fig. 3(a) and starts at $\theta(0) = 90°$ since the initial position of the spacecraft is on the y-axis, as illustrated in Fig. 2.
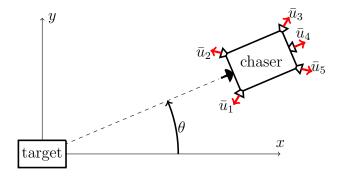
Figure 1: Relative positions and attitudes of the two satellites, with the camera of the chaser always pointing at the target thanks to an independent attitude control system.
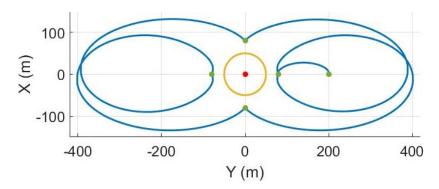

Figure 2: Reference minimal-fuel trajectory (blue) linking the four waypoints (green) to inspect the target satellite (red) without breaching the KOS (yellow).

(a) Orientation of the chaser θ during its mission, with the waypoints in green.

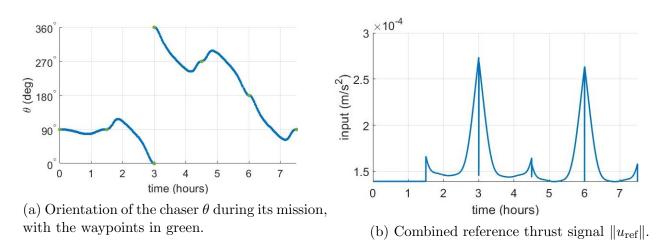(b) Combined reference thrust signal $\|u_{\mathrm{ref}}\|$.

Figure 3: Chaser orientation and thrust profile for the reference trajectory.

When the chaser follows the minimal-fuel reference trajectory of Fig. 2, the resulting thrust profile is represented on Fig. 3(b) and shows several impulses. Their symmetry comes from the symmetry of the reference trajectory of Fig. 2. This thrust profile is obtained from the convex optimization method [17] by propagating dynamics (2) along the fuel-optimal trajectory.

Having described the nominal dynamics and the reference trajectory, we now study the malfunction impacting the chaser. Similarly to what happened to the Nauka module docked to the ISS [7], we assume that an error in the on-board computer of the chaser satellite causes the controller to lose authority over one of the thrusters. The input signal $\bar{u} \in \mathcal{F}(\bar{\mathcal{U}})$ of (2) is then split between the undesirable signal $w \in \mathcal{F}(\mathcal{W})$, $\mathcal{W} = [0, 1]$ and the controlled signal $u \in \mathcal{F}(\mathcal{U})$, $\mathcal{U} = [0, 1]^4$. Matrix $\bar{B}$ is accordingly split into two constant matrices $B \in \mathbb{R}^{4\times4}$ and $C \in \mathbb{R}^4$ so that the dynamics of the malfunctioning satellite become

$$\dot{X}(t) = AX(t) + rR_\theta(t)Bu(t) + rR_\theta(t)Cw(t), \qquad X(0) = X_0 \in \mathbb{R}^4. \qquad (3)$$

We can then formulate our problem of interest.

Problem 1. *With what accuracy can the chaser satellite track the reference trajectory even after enduring a loss of control authority over any one of its thrusters?*

To address Problem 1, we start by determining over which thrusters the spacecraft can resiliently lose control. This investigation is carried out in Section 3 within the resilience framework of [6, 20] based on the 'snap decision rule' of [21] where the controller $u(t)$ has instantaneous knowledge of the state $X(t)$ and of the uncontrolled input $w(t)$. This assumption is lifted in subsequent sections where we study resilient trajectory tracking despite actuation delay.

3 Spacecraft resilience with instantaneous control

We rely on *resilience theory* [20] to determine the thrusters over which the chaser spacecraft can lose control while remaining capable of accomplishing its mission.

3.1 Resilient reachability

Let us first recall the notion of *resilience* from [20] adapted to system (2).

Definition 1. *System* (2) *is* resilient *to the loss of control authority over one of its thrusters if for any target $X_{goal} \in \mathbb{R}^4$ and any undesirable signal $w \in \mathcal{F}(\mathcal{W})$ there exists a control signal $u \in \mathcal{F}(\mathcal{U})$ such that the resulting malfunctioning system* (3) *can reach X_{goal} in finite time.*

Resilience is not automatically sufficient to complete the mission of Problem 1 since Definition 1 only concerns target reachability and not trajectory tracking. However, resilience is necessary for mission completion because tracking is impossible without some degree of reachability. Following the method of [21], to assess the resilience of system (2), we introduce the associated dynamics

$$\dot{X}(t) = AX(t) + rR_\theta(t)p(t), \qquad X(0) = X_0, \qquad p(t) \in \mathcal{P} := B\mathcal{U} \ominus (-C\mathcal{W}), \qquad (4)$$

where $\mathcal{P}$ is the Minkowski difference between the set of controlled inputs $B\mathcal{U} := \{Bu : u \in \mathcal{U}\}$ and the negative of the set of undesirable inputs $-C\mathcal{W} := \{-Cw : w \in \mathcal{W}\}$, i.e., $\mathcal{P} = \{p \in B\mathcal{U} : p - Cw \in B\mathcal{U} \text{ for all } w \in \mathcal{W}\}$. Then, $\mathcal{P}$ represents the amount of control authority remaining after counteracting the worst undesirable input.

According to [22], if systems (2) and (4) were linear, the resilience of system (2) would be equivalent to the controllability of system (4). Let us now define *controllability* in parallel with *stabilizability* as it will be needed later on.

Definition 2. *System* (4) *is* controllable *(resp.* stabilizable*) if for all $X_0 \in \mathbb{R}^4$ and all $X_{goal} \in \mathbb{R}^4$, there exists a time T and a control signal $p \in \mathcal{F}(\mathcal{P})$ driving the state of system* (4) *from $X(0) = X_0$ to $X(T) = X_{goal}$ (resp. to $X(T) = 0$).*

However, nonlinear factor $R_\theta(t)$ in systems (2) and (4) prevents us from immediately applying the resilience results of [21, 22] to these systems. Instead, we provide a partial extension of Hájek's duality theorem [21] to nonlinear dynamics.

Theorem 1. *If system* (4) *is controllable, then system* (2) *is resilient.*

Proof. Let $X_0 \in \mathbb{R}^4$, $X_{goal} \in \mathbb{R}^4$ and $w \in \mathcal{F}(\mathcal{W})$. Since system (4) is controllable, there exists $T \geq 0$ and $p \in \mathcal{F}(\mathcal{P})$ driving the state of system (4) from X_0 to X_{goal} in time T. By definition of $\mathcal{P}$ there exists $u \in \mathcal{F}(\mathcal{U})$ such that $Bu(t) = p(t) - Cw(t)$ for all $t \in [0, T]$. Then, applying input signals u and w to system (3) drives its state from X_0 to X_{goal} in time T. Thus, for all $X_{goal} \in \mathbb{R}^4$ and all $w \in \mathcal{F}(\mathcal{W})$ there exists $u \in \mathcal{F}(\mathcal{U})$ driving malfunctioning system (3) to X_{goal} in finite time, i.e., system (2) is resilient. □

Remark. *The proof of Theorem 1 is actually valid for all nonlinear systems of the form $\dot{x}(t) = f(t, x(t)) + g(t, x(t))\bar{B}\bar{u}(t)$, and not just for system* (2). *The reverse implication of Theorem 1 remains an open question for nonlinear dynamics.*

Relying on Theorem 1, we will now investigate whether system (2) is resilient to a loss of control authority over thruster no. 4. Indeed, this thruster plays a special role in the actuation of the chaser spacecraft due to its location shown on Fig. 1 and yields

$$B = \begin{bmatrix} 0 & 0 & 0 & 0 \\ 0 & 0 & 0 & 0 \\ 1 & 1 & -1 & -1 \\ 1 & -1 & -1 & 1 \end{bmatrix} \quad \text{and} \quad C = \begin{bmatrix} 0 \\ 0 \\ -\sqrt{2} \\ 0 \end{bmatrix}. \tag{5}$$

The polytopes $B\mathcal{U}$ and $-C\mathcal{W}$ are both in $\mathbb{R}^4$, but since they are of dimension 2, we only represent these last two dimensions in Fig. 4. Similarly, the Minkowski difference $\mathcal{P}$ is of dimension 2 and is also illustrated in Fig. 4.
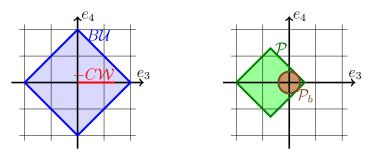

Figure 4: 2D projection of $B\mathcal{U}$ (blue), $-C\mathcal{W}$ (red), their Minkowski difference $\mathcal{P}$ (green) and the largest ball $\mathcal{P}_b$ (brown) centered at 0 that fits inside $\mathcal{P}$ for the case of the loss of control authority over thruster no. 4.

To prove the resilience of system (2) to a loss of control authority over thruster no. 4, we need to verify the controllability of nonlinear system (4). However, this verification of controllability is generally a difficult problem [23]. Instead, we will construct a related linear time-invariant system whose controllability implies that of system (4).

Proposition 1. *System* (2) *is resilient to a loss of control authority over thruster no. 4.*

Proof. Following Theorem 1, we will prove controllability of system (4) to obtain resilience of system (2). Because $-C\mathcal{W} \subseteq \text{int}\,(B\mathcal{U})$, we have $0 \in \text{int}\,(\mathcal{P})$, as seen on Fig. 4. Then, we can define ρ_{max} as the radius of the largest ball of dimension 2 centered at 0 and fitting inside $\mathcal{P}$, i.e., $\rho_{max} := \max\left\{\rho \geq 0 : \mathbb{B}^2(0,\rho) \subseteq \mathcal{P}\right\}$. In our case $\rho_{max} = \sqrt{2} - 1 = 0.414$. Then, the ball $\mathcal{P}_b := \mathbb{B}^2(0, \rho_{max})$ is a subset of $\mathcal{P}$ as illustrated on Fig. 4. Because $\mathcal{P}_b$ is a ball, there is a one-to-one correspondence between inputs $p \in \mathcal{P}_b$ and $R_\theta p \in \mathcal{P}_b$, so the dynamics (4) with inputs constrained to $\mathcal{P}_b$ are in fact
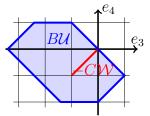
$$\dot{X}(t) = AX(t) + r\hat{B}p(t), \qquad p \in \mathcal{P}_b \subset \mathbb{R}^2, \qquad \hat{B} = \left[\begin{smallmatrix} 0_{2\times2} \\ I_2 \end{smallmatrix}\right]. \tag{6}$$

Because the first two rows of B and C defined in Eq. (5) are null, the geometrical work we completed above only concerns the last two coordinates of the inputs, which explains the structure of matrix $\hat{B}$ in (6). To prove the controllability of system (6), we verify the conditions of Corollary 3.7 of [24]:

- $0 \in \mathcal{P}_b$, so taking $p = 0$ makes $\hat{B}p = 0$;

- the convex hull of $\mathcal{P}_b$ has a non-empty interior in $\mathbb{R}^2$;

- $\left[\hat{B}, A\hat{B}\right] = \left[\begin{smallmatrix} 0_{2\times2} & I_2 \\ I_2 & * \end{smallmatrix}\right]$, so rank $\left(\left[\hat{B}, A\hat{B}\right]\right) = 4$, i.e., the controllability matrix has full rank;

- the real eigenvectors of $A^\top$ are all scalar multiples of $v = (2\Omega, 0, 0, 1)$, which makes $v^\top \hat{B}p = p_2$ for all $p = (p_1, p_2) \in \mathcal{P}_b$ and p_2 can be chosen positive or negative since $\rho_{max} > 0$;

- the eigenvalues of A are $\{0, 0, \pm j\Omega\}$, so they all have a zero real part.

Hence, system (6) is controllable. Because system (4) follows the same dynamics as (6), and has a larger input set encompassing that of system (6), it is also controllable. Then, according to Theorem 1 system (2) is resilient to the loss of control over thruster no. 4. $\qquad\square$

We can now proceed to the case of the other four thrusters. Because of their symmetric placement as shown on Fig. 1, we only need to study one thruster and similar conclusions will hold for the others. For the loss of control authority over thruster no. 1, we represent dimensions 3 and 4 of polytopes $B\mathcal{U}$, $-C\mathcal{W}$, and $\mathcal{P}$ on Fig. 5.
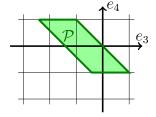

Figure 5: 2D projection of $B\mathcal{U}$ (blue), $-C\mathcal{W}$ (red), and their Minkowski difference $\mathcal{P}$ (green) for the case of the loss of control authority over thruster no. 1.

Note that $(0,0)$ is on the boundary of $\mathcal{P}$, so that $\rho_{max} = 0$, no ball of positive radius centered at 0 can fit inside $\mathcal{P}$. This issue is much more problematic than just preventing us from reusing

the proof of Proposition 1. Indeed, let $\mathcal{T}_{\text{ref}} := \left\{ X_{\text{ref}}(t) : \dot{X}_{\text{ref}}(T) = AX_{\text{ref}} + rR_\theta(t)p_{\text{ref}}(t), \ t \geq 0 \right\}$ be the reference trajectory of Fig. 2, where control law $p_{\text{ref}} \in \mathcal{F}(\mathcal{P}_{\text{ref}})$ is obtained with the trajectory propagation algorithm of [17]. To produce this trajectory, we need $0 \in \text{int}(\mathcal{P}_{\text{ref}})$ as shown on Fig. 6. Since $0 \notin \text{int}(\mathcal{P})$, we have $\mathcal{P}_{\text{ref}} \not\subseteq \mathcal{P}$. Therefore, the spacecraft cannot track $\mathcal{T}_{\text{ref}}$ after the loss of control authority over a thruster other than no. 4.
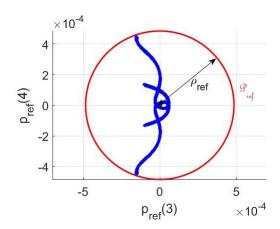

Figure 6: Dimensions 3 and 4 of the reference thrust inputs p_{ref} (blue) included in the ball $\mathcal{P}_{\text{ref}}$ (red) of radius ρ_{ref} (black) for the reference trajectory $\mathcal{T}_{\text{ref}}$.

To simplify further discussions, let us assume that $\mathcal{P}_{\text{ref}}$ is the smallest ball centered at 0 encompassing all $p_{\text{ref}}(t)$, i.e., $\mathcal{P}_{\text{ref}} = \mathbb{B}^2(0, \rho_{\text{ref}})$ with $\rho_{\text{ref}} := \min \left\{ \rho > 0 : p_{\text{ref}}(t) \in \mathbb{B}(0, \rho) \text{ for all } t \geq 0 \right\}$. For the reference trajectory of Fig. 2, radius $\rho_{\text{ref}} = 4.85 \times 10^{-4}$ and is illustrated on Fig. 6.

3.2 Resilient trajectory tracking and robustness to initial state difference

Following the discussion above, we will only investigate resilient trajectory tracking for the loss of control authority over thruster no. 4. In this scenario, $\rho_{max} = 0.414 >> \rho_{\text{ref}} = 4.85 \times 10^{-4}$. Then, the malfunctioning spacecraft has a large amount of control authority left even after counteracting the worst undesirable thrust and producing the reference thrust input. Let us detail why this remaining thrust capability will be sorely needed.

The initial state of the malfunctioning spacecraft X_0 is most likely not exactly equal to $X_{\text{ref}}(0)$, the initial of reference trajectory $\mathcal{T}_{\text{ref}}$, which was designed before the spaceflight. We then need to design a tracking controller with robustness to uncertainty on the initial state. Moreover, if the difference $X_0 - X_{\text{ref}}(0)$ is not actively reduced, it can grow exponentially with time [25]. Thus, we need the extra thrust capability mentioned earlier to counteract $X(t) - X_{\text{ref}}(t)$. Formally, we pick $\varepsilon > 0$ and define input set $\mathcal{P}_\varepsilon := \mathbb{B}^2(0, \varepsilon)$ to overcome $X(t) - X_{\text{ref}}(t)$. For the robust tracking of $\mathcal{T}_{\text{ref}}$ to be admissible, we then need $\mathcal{P}_\varepsilon \oplus \mathcal{P}_{\text{ref}} \subseteq \mathcal{P}$, where we recall $\mathcal{P}$ as the set of control inputs remaining after counteracting the worst undesirable thrust from malfunctioning thruster no. 4. We now introduce the dynamics tasked with counteracting the initial state error

$$\dot{Y}(t) = AY(t) + rR_\theta(t)p_\varepsilon(t), \quad Y(0) = X_0 - X_{\text{ref}}(0), \quad p_\varepsilon(t) \in \mathcal{P}_\varepsilon, \tag{7}$$

where $R_\theta(t)$ is the rotation matrix tracking position $X(t)$ of system (3).

Proposition 2. *If $\varepsilon + \rho_{ref} \leq \rho_{max}$, then system (7) is stabilizable in a finite time t_f and the reference trajectory $\mathcal{T}_{ref}$ can be tracked exactly by system (3) after time t_f, i.e., $X(T) = X_{ref}(T)$ for all $t \geq t_f$.*

Proof. We start with the same trick as in the proof of Proposition 1 by noticing that $\mathcal{P}_\varepsilon = \mathbb{B}^2(0, \varepsilon)$ is left unchanged by the rotation matrix R_θ. Then, system (7) has a one-to-one correspondence with the following linear system

$$\dot{Y}(t) = AY(t) + r\hat{B}p_\varepsilon(t), \quad Y(0) = X_0 - X_{ref}(0), \quad p_\varepsilon(t) \in \mathcal{P}_\varepsilon, \quad \hat{B} = \begin{bmatrix} 0_{2\times 2} \\ I_2 \end{bmatrix}. \tag{8}$$

Since $0 \in \text{int}(\mathcal{P}_\varepsilon)$, $Re(\Lambda(A)) \leq 0$, and $\text{rank}\left(\begin{bmatrix} \hat{B} & A\hat{B} \end{bmatrix}\right) = 4$, Corollary 3.6 of [24] states that system (8) is stabilizable in a finite time t_f and so is system (7) by construction.

Therefore, there exists a signal $p_\varepsilon \in \mathcal{F}(\mathcal{P}_\varepsilon)$ on $[0, t_f]$ yielding $Y(t_f) = 0$ in system (7). Since $0 \in \mathcal{P}_\varepsilon$, we extend the control signal to $p_\varepsilon(t) = 0$ for all $t > t_f$. We now define the control law $p_{track}(t) := p_\varepsilon(t) + p_{ref}(t)$. Note that $\mathcal{P}_\varepsilon \oplus \mathcal{P}_{ref} = \mathbb{B}(0, \varepsilon) \oplus \mathbb{B}(0, \rho_{ref}) = \mathbb{B}(0, \varepsilon + \rho_{ref}) \subseteq \mathbb{B}(0, \rho_{max})$ since $\varepsilon + \rho_{ref} \leq \rho_{max}$. By definition of ρ_{max}, $\mathbb{B}(0, \rho_{max}) \subseteq \mathcal{P}$. Thus, $\mathcal{P}_\varepsilon \oplus \mathcal{P}_{ref} \subseteq \mathcal{P}$, i.e., $p_{track}(t) \in \mathcal{P}$ for all $t \geq 0$.

Let $w \in \mathcal{F}(\mathcal{W})$ be any undesirable input signal. Then, by definition of $\mathcal{P}$, there exists $u \in \mathcal{F}(\mathcal{U})$ such that $Bu(t) = p_{track}(t) - Cw(t)$ for all $t \geq 0$. We now implement this controller for $T \geq t_f$ in system (3):

$$X(T) = e^{AT}\left(X_0 + \int_0^T e^{-At}rR_\theta(t)\big(Bu(t) + Cw(t)\big)\,dt\right)$$

$$= e^{AT}\left(X_0 + \int_0^T e^{-At}rR_\theta(t)\big(p_\varepsilon(t) + p_{ref}(t)\big)\,dt\right)$$

$$= e^{AT}\left(X_0 + \int_0^T e^{-At}rR_\theta(t)p_\varepsilon(t)\,dt + e^{-AT}X_{ref}(T) - X_{ref}(0)\right),$$

because $X_{ref}(T) = e^{AT}\left(X_{ref}(0) + \int_0^T e^{-At}rR_\theta(t)p_{ref}(t)dt\right)$. Then,

$$X(T) - X_{ref}(T) = e^{AT}\left(X_0 - X_{ref}(0) + \int_0^T e^{-At}rR_\theta(t)p_\varepsilon(t)\,dt\right)$$

$$= e^{AT}\left(X_0 - X_{ref}(0) + \int_0^{t_f} e^{-At}rR_\theta(t)p_\varepsilon(t)\,dt\right),$$

since $p_\varepsilon(t) = 0$ for $t > t_f$. By definition of p_ε,

$$Y(t_f) = 0 = e^{At_f}\left(Y(0) + \int_0^{t_f} e^{-At}rR_\theta(t)p_\varepsilon(t)\,dt\right), \quad \text{i.e.,} \quad X_0 - X_{ref}(0) + \int_0^{t_f} e^{-At}rR_\theta(t)p_\varepsilon(t)\,dt = 0.$$

Therefore, $X(T) = X_{ref}(T)$ for all $T \geq t_f$. $\qquad\square$

Proposition 2 states that as long as $\varepsilon + \rho_{ref} \leq \rho_{max}$, there exists a finite time t_f after which any trajectory $\mathcal{T}_{ref}$ can be tracked perfectly despite the loss of control authority over a thruster. Since ε describes the maximal input magnitude of system (7), ε is inversely correlated with its stabilization time t_f. Then, the constraint $\varepsilon + \rho_{ref} \leq \rho_{max}$ yields that the smaller ρ_{ref}, the larger ε and so the smaller t_f is. In other words, the smaller the inputs required to track the reference trajectory, the faster the spacecraft can resume perfect tracking after a loss of control authority. Let us now investigate how the spacecraft would perform if the controller could not react instantly to undesirable thrust inputs.

4 Resilience theory in the presence of actuation delay

In order to account for the unavoidable sensors and thrusters delays on spacecraft [16], we now assume that the controller operates with a constant input delay $\tau > 0$ so that the dynamics of the spacecraft are in fact

$$\dot{X}(t) = AX(t) + rR_\theta(t)Bu\big(t, X(t-\tau), w(t-\tau)\big) + rR_\theta(t)Cw(t), \quad X(0) = X_0 \in \mathbb{R}^4. \quad (9)$$

The controller cannot react immediately to a change of the undesirable input $w(t)$ and cancel it instantaneously as in Section 3. Only starting at $t + \tau$ can the controller try to counteract $Cw(t)$. However, at time $t + \tau$ the effect of $w(t)$ on the state $X(t+\tau)$ has become $e^{A\tau}Cw(t)$. Hence, set $\mathcal{P}$ introduced in (4) does not describe the remaining control authority anymore.

To study whether the more realistic spacecraft dynamics (9) can resiliently track a reference trajectory, we first need to establish several novel theoretical results. Indeed, resilience in the presence of actuation delay has never been investigated before. We first want to establish general results, before specializing them to dynamics (9). Let us first work on general linear systems with input delay and no rotation R_θ. The rotation matrix would only obfuscate the already complex theory of resilience in the presence of actuation delay.

4.1 Framework for actuation delay

We study a linear system of initial dynamics $\dot{x}(t) = Ax(t) + \bar{B}\bar{u}(t)$ with $x(0) = x_0 \in \mathbb{R}^n$, $\bar{u}(t) \in \bar{\mathcal{U}}$ an hyperrectangle in $\mathbb{R}^{m+q}$ and $A \in \mathbb{R}^{n \times n}$, $\bar{B} \in \mathbb{R}^{n \times (m+q)}$ constant matrices. Similarly to the motivating spacecraft scenario, this system suffers a loss of control authority over q of its initial $m + q$ actuators, and the controller is further inflicted with a constant actuation delay $\tau > 0$. We split the signal $\bar{u}$ into its controlled part $u \in \mathcal{F}(\mathcal{U})$ and its uncontrolled part $w \in \mathcal{F}(\mathcal{W})$ with $\mathcal{U}$ and $\mathcal{W}$ hyperrectangles in $\mathbb{R}^m$ and $\mathbb{R}^q$ respectively. Matrix $\bar{B}$ is accordingly split into $B \in \mathbb{R}^{n \times m}$ and $C \in \mathbb{R}^{n \times q}$ such that the dynamics of the malfunctioning system are

$$\dot{x}(t) = Ax(t) + Cw(t) + Bu\big(t, x(t-\tau), w(t-\tau)\big), \quad x(0) = x_0 \in \mathbb{R}^n, \quad u(t) \in \mathcal{U}, \quad w(t) \in \mathcal{W}. \quad (10)$$

We want to establish conditions under which system (10) can resiliently reach a target set.

Definition 3. *A convex set $\mathcal{G} \subseteq \mathbb{R}^n$ is* resiliently reachable *at time T from x_0 by system* (10) *if for all undesirable inputs $w \in \mathcal{F}(\mathcal{W})$ there exists a control signal $u \in \mathcal{F}(\mathcal{U})$ such that $u(t) = u\big(t, x(t-\tau), w(t-\tau)\big)$ and $x(T) \in \mathcal{G}$.*

Generalizing works [21, 20] we introduce the family of sets $\mathcal{P}_t := B\mathcal{U} \ominus (-e^{At}C\mathcal{W})$ for all $t \geq 0$ with $e^{At}C\mathcal{W} := \big\{e^{At}Cw : w \in \mathcal{W}\big\}$. We will show that $\mathcal{P}_\tau$ is the set of actual control inputs of system (10), when u has canceled any undesirable input w with a delay τ. Set $\mathcal{P}_\tau$ is the time delayed extension of $\mathcal{P}$ from (4).

Definition 4. *The* minimal correction time T_c *represents the minimal time after which any undesirable input can be counteracted, $T_c := \inf\big\{t \geq \tau : \mathcal{P}_t \neq \emptyset\big\}$.*

If $T_c = +\infty$, then the impact on the state of some undesirable inputs cannot be canceled by any control input after the actuation delay, i.e., there exists some $w \in \mathcal{W}$ such that $-e^{At}Cw \notin B\mathcal{U}$ for all $t \geq \tau$. In this case, resilient reachability is impossible [22]. Let us now assume that T_c is finite in order to build the theory for resilience in the presence of actuation delay.

4.2 Resilient reachability despite actuation delay

We want to know whether a target set $\mathcal{G} \subseteq \mathbb{R}^n$ is resiliently reachable by system (10). Because of the actuation delay τ, the controller can only guarantee that $x(t)$ is in some neighborhood of $x(t - \tau)$, it cannot ensure an exact location. Then, set $\mathcal{G}$ needs a minimal radius $\rho > 0$ to be resiliently reachable. Inspired by Hájek's approach [21], we introduce system (11) as a counterpart to system (10), just like system (4) was the counterpart of system (3) for the spacecraft without actuation delay.

$$\dot{x}(t) = Ax(t) + p(t), \quad x(0) = e^{AT_c}x_0, \quad p(t) \in \mathcal{P}_{T_c} := B\mathcal{U} \ominus (-e^{AT_c}C\mathcal{W}). \tag{11}$$

Note that the input p of system (11) does not suffer from actuation delay by design of $\mathcal{P}_{T_c}$.

Theorem 2. *If there exists $x_g \in \mathcal{G}$ such that $\mathbb{B}(x_g, \rho) \subseteq \mathcal{G}$ and x_g is reachable in a finite time T by system (11), then $\mathcal{G}$ is resiliently reachable by system (10) in time $T + T_c$, with $\rho := \frac{c}{\mu(A)}\big(e^{\mu(A)T_c} - 1\big)$ and $c := \max\big\{\|Cw\| : w \in \mathcal{W}\big\}$.*

Proof. We first introduce the log-norm of matrix A defined in [26] as $\mu(A) := \max\big\{\Lambda((A + A^\top)/2)\big\}$. Then, $\|e^{At}\| \leq e^{\mu(A)t}$ for all $t \geq 0$ according to. Since T is the time at which system (11) can reach x_g from $e^{AT_c}x_0$, there exists $p(s) \in \mathcal{P}_{T_c}$ for all $s \in [0, T]$ such that

$$x_g = x(T) = e^{AT}\left(e^{AT_c}x_0 + \int_0^T e^{-As}p(s)\,ds\right), \quad \text{i.e.,} \quad e^{AT}\int_0^T e^{-As}p(s)\,ds = x_g - e^{A(T+T_c)}x_0.$$

Let $w \in \mathcal{F}(\mathcal{W})$ be some undesirable input affecting system (10). We now define the corresponding control input $u \in \mathcal{F}(\mathcal{U})$ so that it satisfies: $Bu(t) = 0$ for $t \in [0, T_c]$ and $Bu(t) = p(t - T_c) - e^{AT_c}Cw(t - T_c)$ for $t \in [T_c, T + T_c]$. Note that $u(t) \in \mathcal{U}$ by definition of $p(t) \in \mathcal{P}_{T_c}$. We apply this control law to system (10):

$$x(T + T_c) = e^{A(T+T_c)}\left(x_0 + \int_0^{T+T_c} e^{-At}Cw(t)\,dt + \int_0^{T+T_c} e^{-At}Bu(t)dt\right)$$

$$= e^{A(T+T_c)}\left(x_0 + \int_0^{T+T_c} e^{-At}Cw(t)\,dt + \int_{T_c}^{T+T_c} e^{-At}\big(p(t - T_c) - e^{AT_c}Cw(t - T_c)\big)dt\right)$$

$$= e^{A(T+T_c)}\left(x_0 + \int_0^{T+T_c} e^{-At}Cw(t)\,dt + \int_0^T e^{-A(s+T_c)}\big(p(s) - e^{AT_c}Cw(s)\big)ds\right)$$

$$= e^{A(T+T_c)}\left(x_0 + \int_T^{T+T_c} e^{-At}Cw(t)dt\right) + e^{AT}\int_0^T e^{-As}p(s)ds$$

$$= e^{A(T+T_c)}x_0 + \int_0^{T_c} e^{As}Cw(T + T_c - s)ds + \big(x_g - e^{A(T+T_c)}x_0\big)$$

$$= x_g + \int_0^{T_c} e^{As}Cw(T + T_c - s)ds,$$

thanks to the definition of $p(s) \in \mathcal{P}_{T_c}$. Then, by subtracting x_g and using the triangle inequality we obtain

$$\big\|x(T + T_c) - x_g\big\| \leq \int_0^{T_c} \big\|e^{As}\big\| \big\|Cw(T + T_c - s)\big\|ds \leq \int_0^{T_c} e^{\mu(A)s}c\,ds = \frac{c}{\mu(A)}\big(e^{\mu(A)T_c} - 1\big) = \rho.$$

Since $\mathbb{B}(x_g, \rho) \subseteq \mathcal{G}$, we have $x(T + T_c) \in \mathcal{G}$. Hence, $\mathcal{G}$ is resiliently reachable by system (10) in time $T + T_c$. $\qquad\square$

Note that the control $p(t - T_c)$ responsible for steering to x_g in Theorem 2 is in fact an *open loop* control. A *feedback control* may perform better in practice, but the saturation enforcing that such signal remains bounded in $\mathcal{P}_{T_c}$ leads to a substantial increase in complexity, as demonstrated in Section 5.2.

Theorem 2 provides a sufficient resilient reachability condition for delayed system (10) in terms of the reachability of $\mathcal{G}$ by system (11). In turn, a sufficient condition for this last property can be verified with the lemma below.

Lemma 1. *Let $P \in \mathbb{R}^{n \times d}$ be a matrix whose columns are d linearly independent vectors of $\mathcal{P}_{T_c}$ with $d := \dim(\mathcal{P}_{T_c}) \geq 0$. If $0 \in \text{int}(\mathcal{P}_{T_c})$, then system (11) is controllable if and only if $Re(\Lambda(A)) = 0$, $\text{rank}(\mathcal{C}(A, P)) = n$, and there is no real eigenvector v of $A^\top$ satisfying $v^\top p \leq 0$ for all $p \in \mathcal{P}_{T_c}$.*

Proof. By construction, $\text{Im}(P) = \text{span}(\mathcal{P}_{T_c})$ so that $\mathcal{C}(A, P)$ is a controllability matrix associated with system (11). Since $\mathcal{U}$ and $\mathcal{W}$ are convex, so are $B\mathcal{U}$ and $e^{AT_c}C\mathcal{W}$. Their Minkowski difference $\mathcal{P}_{T_c}$ is then also convex [27]. Then, $0 \in \text{int}(\text{co}(\mathcal{P}_{T_c}))$ and trivially $0 \in \text{Ker}(I_n) \cap \mathcal{P}_{T_c}$. These two inclusions allow us to apply Corollary 3.7 of [24] which yields the controllability condition. $\square$

Thus, combining Lemma 1 and Theorem 2 provides a sufficient condition for resilient reachability in the presence of actuation delay. We will now investigate the more complicated problem of resilient trajectory tracking despite actuation delay.

4.3 Resilient trajectory tracking despite actuation delay

We want system (10) to track the actuated reference trajectory $\mathcal{T}_{\text{ref}}$ designed for system (11) by $\mathcal{T}_{\text{ref}} := \{x_{\text{ref}}(t) : \dot{x}_{\text{ref}}(t) = Ax_{\text{ref}}(t) + p_{\text{ref}}(t), \text{ for all } t \geq 0\}$ with $p_{\text{ref}} \in \mathcal{F}(\mathcal{P}_{\text{ref}})$. We also define $\mathcal{P}_\varepsilon$ as a compact set of $\mathbb{R}^n$ satisfying $0 \in \text{relint}(\mathcal{P}_\varepsilon)$ and $\dim(\mathcal{P}_\varepsilon) = n$. As in Section 3.2, we use input set $\mathcal{P}_\varepsilon$ to counteract the error arising from $x_0 \neq x_{\text{ref}}(0)$ through the dynamics

$$\dot{y}(t) = Ay(t) + p_\varepsilon(t), \quad y(0) = e^{AT_c}(x_0 - x_{\text{ref}}(0)), \quad p_\varepsilon(t) \in \mathcal{P}_\varepsilon. \tag{12}$$

We can then state our resilient trajectory tracking result.

Theorem 3. *If $\mathcal{P}_\varepsilon \oplus \mathcal{P}_{\text{ref}} \subseteq \mathcal{P}_{T_c}$ and system (12) is stabilizable in a finite time t_f, then the reference trajectory $\mathcal{T}_{\text{ref}}$ can be tracked by system (10) with a precision ρ after time $t_f + T_c$, i.e., $\|x(T) - x_{\text{ref}}(T)\| \leq \rho$ for all $T \geq t_f + T_c$.*

Proof. Since system (12) is stabilizable in a finite time t_f, there exists a signal $p_\varepsilon(t) \in \mathcal{P}_\varepsilon$ for all $t \in [0, t_f]$ yielding $y(t_f) = 0$. Because $0 \in \mathcal{P}_\varepsilon$, we can extend signal p_ε with $p_\varepsilon(t) = 0$ for all $t > t_f$. Let $w \in \mathcal{F}(\mathcal{W})$ be the undesirable input signal. Since $\mathcal{P}_\varepsilon \oplus \mathcal{P}_{\text{ref}} \subseteq \mathcal{P}_{T_c} = B\mathcal{U} \ominus (-e^{AT_c}C\mathcal{W})$, there exists $u \in \mathcal{F}(\mathcal{U})$ such that $Bu(t) = p_{\text{ref}}(t) + p_\varepsilon(t - T_c) - e^{AT_c}Cw(t - T_c)$ for $t \geq T_c$. Indeed, the reference trajectory is known ahead of time, so $u(t)$ has access to $p_{\text{ref}}(t)$. We define u to satisfy $Bu(t) = p_{\text{ref}}(t)$ for $t \in [0, T_c]$. We now implement this controller for $T \geq T_c$ in system (10)

$$x(T) = e^{AT}\left(x_0 + \int_0^{T_c} e^{-At}Bu(t)\,dt + \int_{T_c}^T e^{-At}Bu(t)\,dt + \int_0^T e^{-At}Cw(t)\,dt\right)$$

$$= e^{AT}\left(x_0 + \int_0^{T_c} e^{-At}p_{\text{ref}}(t)\,dt + \int_{T_c}^T e^{-At}\left(p_{\text{ref}}(t) + p_\varepsilon(t - T_c) - e^{AT_c}Cw(t - T_c)\right)dt + \int_0^T e^{-At}Cw(t)\,dt\right)$$

$$= e^{AT}\left(x_0 + \int_0^T e^{-At}p_{\text{ref}}(t)\,dt + \int_0^{T-T_c} e^{-As}\left(e^{-AT_c}p_\varepsilon(s) - Cw(s)\right)ds + \int_0^T e^{-At}Cw(t)\,dt\right)$$

$$= e^{AT}\left(x_0 + e^{-AT}x_{\text{ref}}(T) - x_{\text{ref}}(0) + e^{-AT_c}\int_0^{T-T_c} e^{-As}p_\varepsilon(s)\,ds + \int_{T-T_c}^T e^{-At}Cw(t)\,dt\right),$$

12

by definition of p_{ref}. Then,

$$x(T) - x_{\text{ref}}(T) = e^{A(T-T_c)} \left(e^{AT_c}\big(x_0 - x_{\text{ref}}(0)\big) + \int_0^{T-T_c} e^{-As} p_\varepsilon(s)\,ds \right) + \int_0^{T_c} e^{As} Cw(T-s)\,ds. \quad (13)$$

Note that the last integral term is the same as in Theorem 2 and hence can be bounded similarly:

$$\left\| \int_0^{T_c} e^{As} Cw(T-s)\,ds \right\| \leq \int_0^{T_c} \left\| e^{As} \right\| \left\| Cw(T-s) \right\| ds \leq c \int_0^{T_c} e^{\mu(A)s} ds = \rho.$$

Since p_ε stabilizes system (12) in time t_f, we have $y(T) = 0$ for all $T \geq t_f$. In particular, for $T \geq t_f + T_c$ we obtain $y(T - T_c) = 0 = e^{A(T-T_c)}\left(y(0) + \int_0^{T-T_c} e^{-As} p_\varepsilon(s)\,ds \right)$. Note that $y(T - T_c)$ is exactly the central term in (13), which finally yields $\left\| x(T) - x_{\text{ref}}(T) \right\| \leq \rho$. $\qquad\square$

Without control signal p_ε, the tracking error would be $\|x(t) - x_{\text{ref}}(t)\| \leq \rho + \left\| e^{At}\big(x_0 - x_{\text{ref}}(0)\big) \right\|$, which can grow exponentially if $x_0 - x_{\text{ref}}(0)$ is collinear with a positive eigenvector of A. When $x_0 = x_{\text{ref}}(0)$, we do not need p_ε and the tracking can be performed with precision ρ from time T_c onward.

Theorem 3 provides a sufficient condition for resilient trajectory tracking by delayed system (10) in terms of the finite time stabilizability of system (12). In turn, this property can be verified with the lemma below.

Lemma 2. *Let $P_\varepsilon \in \mathbb{R}^{n \times d}$ be a matrix whose columns are d linearly independent vectors of $\mathcal{P}_\varepsilon$, with $d = \dim(\mathcal{P}_{T_c}) = \dim(\mathcal{P}_\varepsilon)$. System (12) is stabilizable in a finite time if and only if $Re(\Lambda(A)) \leq 0$, $\mathrm{rank}(\mathcal{C}(A, P_\varepsilon)) = n$ and there is no real eigenvector v of $A^\top$ satisfying $v^\top p \leq 0$ for all $p \in \mathcal{P}_\varepsilon$.*

Proof. By construction $\mathrm{Im}(P_\varepsilon) = \mathrm{span}(\mathcal{P}_\varepsilon)$, so that $\mathcal{C}(A, P_\varepsilon)$ is a controllability matrix associated with system (12). We made the assumption that $0 \in \mathrm{relint}(\mathcal{P}_\varepsilon)$, so we can apply Proposition 2 of [22] which guarantees that system (12) is stabilizable in finite time. $\qquad\square$

Now that we have established sufficient conditions for resilient reachability and resilient trajectory tracking for linear systems in the presence of actuation delay, we will investigate how to adapt this theory to the spacecraft dynamics (9).

5 Spacecraft resilience in the presence of actuation delay

In this section we extend the linear theory of Section 4 to the rotating dynamics (9) to build an answer to Problem 1. We start by verifying whether the open-loop controller of Section 4.3 can be applied to the spacecraft.

5.1 Open-loop controller

To adapt the resilient trajectory tracking controller of Theorem 3 to nonlinear system (9), we need to modify the minimal correction time T_c introduced for linear systems in Definition 4. However, we will show that such a modification is in fact impossible and prevents a straightforward extension of Theorem 3 to nonlinear system (9). If we were to adapt T_c to system (9), we need to understand the reasoning behind Definition 4, which comes from the calculations of Theorem 3, where T_c allows $Bu(T)$ to counteract the effect of $w(T - T_c)$ on the state $x(T)$. We will then emulate the proof of Theorem 3 for nonlinear dynamics (9) in the vain hope of determining an updated T_c.

The reference trajectory is $\mathcal{T}_{\text{ref}} = \{X_{\text{ref}}(t) : \dot{X}_{\text{ref}}(t) = AX_{\text{ref}}(t) + rp_{\text{ref}}(t)$ for all $t \geq 0\}$, $p_{\text{ref}} \in \mathcal{F}(\mathcal{P}_{\text{ref}})$ with $\mathcal{P}_{\text{ref}} = \mathbb{B}^2(0, \rho_{\text{ref}})$. Inspired by Theorem 3, for $w \in \mathcal{F}(\mathcal{W})$ we define the control law $Bu(t) = R_\theta^{-1}(t)p_{\text{ref}}(t)$ for $t \in [0, T_c]$ and $Bu(t) = R_\theta^{-1}(t)p_{\text{ref}}(t) + p_\varepsilon(t - T_c) + Bu_w(t - T_c)$ for $t \geq T_c$, where p_ε should counteract the error arising from $X_0 - X_{\text{ref}}(0)$ and Bu_w should cancel the effect of w. We apply this control law to the spacecraft dynamics (9) for $T \geq T_c$:

$$
\begin{aligned}
X(T) &= e^{AT}\left(X_0 + \int_0^T e^{-At}rR_\theta(t)\big(Bu(t) + Cw(t)\big)dt\right) \\
&= e^{AT}\left(X_0 + \int_0^T e^{-At}rp_{\text{ref}}(t)dt + \int_{T_c}^T e^{-At}rR_\theta(t)\big(p_\varepsilon(t - T_c) + Bu_w(t - T_c)\big)dt + \int_0^T e^{-At}rR_\theta(t)Cw(t)dt\right) \\
&= e^{AT}\left(X_0 + e^{-AT}X_{\text{ref}}(T) - X_{\text{ref}}(0) + \int_0^{T-T_c} e^{-A(t+T_c)}rR_\theta(t + T_c)\big(p_\varepsilon(t) + Bu_w(t)\big)dt\right) \\
&\quad + \int_0^T e^{A(T-t)}rR_\theta(t)Cw(t)dt \\
&= X_{\text{ref}}(T) + e^{A(T-T_c)}\left(e^{AT_c}\big(X_0 - X_{\text{ref}}(0)\big) + \int_0^{T-T_c} e^{-A(t+T_c)}rR_\theta(t + T_c)p_\varepsilon(t)\right) \\
&\quad + \int_{T-T_c}^T e^{A(T-t)}rR_\theta(t)Cw(t)dt + e^{AT}\int_0^{T-T_c} e^{-At}r\big[R_\theta(t)Cw(t) + e^{-AT_c}R_\theta(t + T_c)Bu_w(t)\big]dt.
\end{aligned}
$$

The last term in square brackets is the one to be canceled by the appropriate choice of Bu_w and leads to the updated definition

$$T_c = \inf\left\{T \geq \tau : -R_\theta^{-1}(t + T)e^{AT}R_\theta(t)C\mathcal{W} \subseteq B\mathcal{U} \text{ for all } t \geq 0\right\}. \tag{14}$$

However, this definition of T_c creates a circular dependency on $R_\theta(t)$, which depends on state $X(t)$, which is in turn modified by controller u which relies on T_c. Then, (14) properly defines T_c only if it is invariant with respect to $\theta(t)$. Let us investigate this question by calculating $R_\theta^{-1}(t + T)e^{AT}R_\theta(t)C$.

Recall that

$$
A = \begin{bmatrix} 0 & 0 & 1 & 0 \\ 0 & 0 & 0 & 1 \\ 3\Omega^2 & 0 & 0 & 2\Omega \\ 0 & 0 & -2\Omega & 0 \end{bmatrix},
$$

and we can easily verify the two simple recursions: $A^{2n+2} = (-1)^n\Omega^{2n}A^2$ and $A^{2n+3} = (-1)^n\Omega^{2n}A^3$ for all $n \in \mathbb{N}$, with

$$
A^2 = \begin{bmatrix} 3\Omega^2 & 0 & 0 & 2\Omega \\ 0 & 0 & -2\Omega & 0 \\ 0 & 0 & -\Omega^2 & 0 \\ -6\Omega^3 & 0 & 0 & -4\Omega^2 \end{bmatrix} \quad \text{and} \quad A^3 = \begin{bmatrix} 0 & 0 & -\Omega^2 & 0 \\ -6\Omega^3 & 0 & 0 & -4\Omega^2 \\ -3\Omega^4 & 0 & 0 & -2\Omega^3 \\ 0 & 0 & 2\Omega^3 & 0 \end{bmatrix}.
$$

With these relations we can calculate the exponential series:

$$
\begin{aligned}
e^{At} - I - At &= \sum_{n=2}^{+\infty} A^n \frac{t^n}{n!} = \sum_{n=0}^{+\infty} A^{2n+2} \frac{t^{2n+2}}{(2n+2)!} + \sum_{n=0}^{+\infty} A^{2n+3} \frac{t^{2n+3}}{(2n+3)!} \\
&= \sum_{n=0}^{+\infty} (-1)^n \Omega^{2n} A^2 \frac{t^{2n+2}}{(2n+2)!} + \sum_{n=0}^{+\infty} (-1)^n \Omega^{2n} A^3 \frac{t^{2n+3}}{(2n+3)!} \\
&= -\frac{A^2}{\Omega^2} \sum_{n=0}^{+\infty} (-1)^{n+1} \frac{(\Omega t)^{2n+2}}{(2n+2)!} - \frac{A^3}{\Omega^3} \sum_{n=0}^{+\infty} (-1)^{n+1} \frac{(\Omega t)^{2n+3}}{(2n+3)!} \\
&= -\frac{A^2}{\Omega^2} \big(\cos(\Omega t) - 1 \big) - \frac{A^3}{\Omega^3} \big(\sin(\Omega t) - \Omega t \big) = \frac{A^2}{\Omega^2} \big(1 - \cos(\Omega t) \big) + \frac{A^3}{\Omega^3} \big(\Omega t - \sin(\Omega t) \big).
\end{aligned}
$$

Then, replacing A, A^2 and A^3 in the equation above, we obtain:

$$
e^{At} = \begin{bmatrix}
4 - 3\cos(\Omega t) & 0 & \frac{1}{\Omega} \sin(\Omega t) & \frac{2}{\Omega} \big(1 - \cos(\Omega t) \big) \\
6\big(\sin(\Omega t) - \Omega t \big) & 1 & \frac{2}{\Omega} \big(\cos(\Omega t) - 1 \big) & -3t + \frac{4}{\Omega} \sin(\Omega t) \\
3\Omega \sin(\Omega t) & 0 & \cos(\Omega t) & 2\sin(\Omega t) \\
6\Omega \big(\cos(\Omega t) - 1 \big) & 0 & -2\sin(\Omega t) & 4\cos(\Omega t) - 3
\end{bmatrix}.
$$

After the loss of control authority over thruster no. 4, matrices B and C are defined in (5). Then,

$$
e^{At}C = -\sqrt{2} \begin{bmatrix}
\sin(\Omega t)/\Omega \\
2\big(\cos(\Omega t) - 1 \big)/\Omega \\
\cos(\Omega t) \\
-2\sin(\Omega t)
\end{bmatrix}.
$$

Since the first two rows of B are null, to have $-R_\theta^{-1}(t + T_c) e^{AT_c} R_\theta(t) C \mathcal{W} \subseteq B\mathcal{U}$, the first two components of $-R_\theta^{-1}(t + T_c) e^{AT_c} R_\theta(t) C$ should also be zero for all $t \geq 0$, i.e.,

$$
0 = \cos\big(\theta(t)\big) \sin(\Omega T_c) + 2\sin\big(\theta(t)\big)\big(1 - \cos(\Omega T_c)\big), \tag{15}
$$

$$
0 = 2\cos\big(\theta(t)\big)\big(\cos(\Omega T_c) - 1\big) + \sin\big(\theta(t)\big)\big(4\sin(\Omega T_c) - 3\Omega T_c\big). \tag{16}
$$

For (15) to hold independently of $\theta(t)$, we need $\sin(\Omega T_c) = 0$ and $\cos(\Omega T_c) = 1$, i.e., $T_c = \frac{2\pi}{\Omega} n$, $n \in \mathbb{N}$. However, (16) would yield $\sin\big(\theta(t)\big) = 0$, i.e., $y(t) = 0$ for all $t \geq 0$ which prevents the spacecraft from tracking trajectory $\mathcal{T}_{\text{ref}}$. Therefore, we cannot define a minimal correction time T_c for the nonlinear spacecraft dynamics (9). Then, we cannot cancel exactly $Cw(t)$ after some actuation delay as we did in Section 4.3. Without this perfect cancellation an open-loop controller like in Theorem 3 would not be able to track a trajectory. We will then transform this controller into a more complex feedback controller.

5.2 Closed-loop controller

Motivated by the ISS malfunction [7] where the undesirable thrust was constant, we will assume in this section that w is Lipschitz continuous. As in Theorem 3 we partition $\mathcal{P} = B\mathcal{U} \ominus -C\mathcal{W}$ into two parts: $\mathcal{P}_{\text{ref}}$ for the trajectory tracking and $\mathcal{P}_\varepsilon$ for the feedback correction. However, $u(t)$ has only access to $X(t - \tau)$ and not $X(t)$, hence a straightforward linear feedback is not possible. We will replace $X(t)$ by a state predictor $X_p(t)$, designed to predict $X(t)$ based on the information

15

available at time $t - \tau$. We will use a predictor adapted from [28] which takes advantage of the system's dynamics:

$$X_p(t) = e^{A\tau} X(t - \tau) + \int_{t-\tau}^{t} e^{A(t-s)} r R_\theta(s) \big(B u(s) + C w(s - \tau) \big) ds. \tag{17}$$

Before stating our main theorem for resilient trajectory tracking, we recall the definitions of ρ_{max} from Proposition 1, $\rho_{max} = \max \big\{ \rho \geq 0 : \mathbb{B}^2(0, \rho) \subseteq \mathcal{P} \big\}$, and the log-norm $\mu(A) = \max \big\{ \Lambda((A + A^\top)/2) \big\}$.

Theorem 4. *Let $K \in \mathbb{R}^{4 \times 4}$ such that $\tilde{A} := A - rBK$ is Hurwitz, and let $P \in \mathbb{R}^{4 \times 4}$ and $Q \in \mathbb{R}^{4 \times 4}$ such that $P \succ 0$, $Q \succ 0$ and $\tilde{A}^\top P + P \tilde{A} = -Q$. Define $\alpha := \frac{\lambda_{min}^Q}{2\lambda_{max}^P}$, $\beta := r \sqrt{\lambda_{max}^P} \|C\| L \tau$, and $\gamma := r \|BK\| \frac{e^{\mu(A)\tau} - 1}{\mu(A)}$. For $L > 0$, let $\varepsilon := \frac{\|BK\|}{\sqrt{\lambda_{min}^P}} \max \left(\|X_{ref}(0) - X(0)\|_P, \frac{\beta}{\alpha}(1 + \gamma) \right) + \gamma \|C\| L \tau$.*

If $\varepsilon + \rho_{ref} \leq \rho_{max}$, then, for all $w \in \mathcal{F}(\mathcal{W})$ with a Lipschitz constant L, the malfunctioning spacecraft (9) can track reference trajectory $\mathcal{T}_{ref}$ with a tolerance $\|X_{ref}(t) - X(t)\| \leq \frac{1}{\sqrt{\lambda_{min}^P}} \max \left(\|X_{ref}(0) - X(0)\|_P, \frac{\beta}{\alpha}(1 + \gamma) \right)$ for all $t \geq \tau$.

Proof. The existence of matrix K is justified by the controllability of the pair (A, B) [25]. Since the resulting $\tilde{A}$ is Hurwitz, matrices $P \succ 0$ and $Q \succ 0$ exist according to Lyapunov theory [29]. We consider any $w \in \mathcal{F}(\mathcal{W})$ with a Lipschitz constant L and assume that $\varepsilon + \rho_{ref} \leq \rho_{max}$. We define $\mathcal{P}_\varepsilon := \mathbb{B}^2(0, \varepsilon)$ and recall $\mathcal{P}_b = \mathbb{B}^2(0, \rho_{max})$ as introduced in Proposition 1. Then, $\mathcal{P}_\varepsilon \oplus \mathcal{P}_{ref} = \mathbb{B}^2(0, \varepsilon) \oplus \mathbb{B}^2(0, \rho_{ref}) = \mathbb{B}^2(0, \varepsilon + \rho_{ref}) \subseteq \mathbb{B}^2(0, \rho_{max}) = \mathcal{P}_b \subseteq \mathcal{P}$.

For $t \geq \tau$ we introduce control signals u_w, u_{ref} and u_ε such that $Bu_w(t) := -Cw(t - \tau)$, $Bu_{ref}(t) := R_\theta^{-1}(t) p_{ref}(t)$ and $Bu_\varepsilon(t) := R_\theta^{-1}(t) BK \big(X_{ref}(t) - X_p(t) \big)$ with the predictor X_p from (17). We consequently define the feedback control law u by

$$Bu(t) := Bu_w(t) + Bu_{ref}(t) + Bu_\varepsilon(t) = -Cw(t - \tau) + R_\theta^{-1}(t) p_{ref}(t) + R_\theta^{-1}(t) BK \big(X_{ref}(t) - X_p(t) \big). \tag{18}$$

To prove that controller (18) is admissible we need to show that $Bu(t) \in B\mathcal{U}$ for all $t \geq \tau$. Firstly, $Bu_w(t) = -Cw(t - \tau) \in -C\mathcal{W}$. Because $\mathcal{P}_{ref}$ is a ball centered on 0, it is invariant by rotation R_θ. Then, $R_\theta^{-1}(t) p_{ref}(t) \in \mathcal{P}_{ref}$, i.e., $Bu_{ref}(t) \in \mathcal{P}_{ref}$. Since $-C\mathcal{W} \oplus \mathcal{P}_{ref} \oplus \mathcal{P}_\varepsilon \subseteq B\mathcal{U}$, it now suffices to show that $Bu_\varepsilon(t) \in \mathcal{P}_\varepsilon = \mathbb{B}^2(0, \varepsilon)$. To do so, we first apply (18) to dynamics (9). By definition of $\mathcal{T}_{ref}$, we have $r p_{ref}(t) = \dot{X}_{ref}(t) - AX_{ref}(t)$, and thus

$$\dot{X}(t) = AX(t) + rR_\theta(t) Bu(t) + rR_\theta(t) Cw(t)$$
$$= AX(t) - rR_\theta(t) Cw(t - \tau) + \dot{X}_{ref}(t) - AX_{ref}(t) + rBK \big(X_{ref}(t) - X_p(t) \big) + rR_\theta(t) Cw(t),$$

i.e.,

$$\dot{X}(t) - \dot{X}_{ref}(t) = (A - rBK) \big(X(t) - X_{ref}(t) \big) + rR_\theta(t) \big(Cw(t) - Cw(t - \tau) \big) + rBK \big(X(t) - X_p(t) \big).$$

We define

$$Y(t) := X(t) - X_{ref}(t), \quad \Delta C(t) := rR_\theta(t) \big(Cw(t) - Cw(t - \tau) \big), \quad \Delta X(t) := rBK \big(X(t) - X_p(t) \big),$$

so that $\dot{Y}(t) = \tilde{A} Y(t) + \Delta C(t) + \Delta X(t)$. Inspired by the method described in Section 9.3 of [25], we will now show that $Y(t)$ is bounded, which in turn will prove that $Bu_\varepsilon(t) \in \mathcal{P}_\varepsilon$ and hence that

control law (18) is admissible. We consider the derivative of the norm $Y(t)^\top P Y(t) = \|Y(t)\|_P^2$ and obtain the following:

$$\frac{d}{dt}\|Y(t)\|_P^2 = \dot{Y}(t)^\top P Y(t) + Y(t)^\top P\dot{Y}(t) = Y(t)^\top\big(\tilde{A}^\top P + P\tilde{A}\big)Y(t) + 2Y(t)^\top P\big(\Delta C(t) + \Delta X(t)\big).$$

Since $\|\cdot\|_P$ is a norm, the Cauchy-Schwarz inequality [30] yields $Y(t)^\top P\Delta C(t) \leq \|Y(t)\|_P\|\Delta C(t)\|_P$. Then, using $\|R_\theta(t)\| = 1$ and the Lipschitz constant L of w, we have

$$\|\Delta C(t)\|_P \leq \sqrt{\lambda_{max}^P}\,r\|R_\theta(t)\|\|Cw(t) - Cw(t-\tau)\| \leq r\sqrt{\lambda_{max}^P}\|C\|\big|w(t) - w(t-\tau)\big|$$
$$\leq r\sqrt{\lambda_{max}^P}\|C\|L\tau = \beta.$$

Similarly,

$$\|\Delta X(t)\|_P \leq r\sqrt{\lambda_{max}^P}\big\|BK\big(X(t) - X_p(t)\big)\big\| \leq r\sqrt{\lambda_{max}^P}\|BK\|\|X(t) - X_p(t)\|.$$

We write the state of the system $X(t)$ in a form similar to (17) to compare it with X_p:

$$X(t) = e^{A\tau}X(t-\tau) + \int_{t-\tau}^t e^{A(t-s)}rR_\theta(s)\big(Bu(s) + Cw(s)\big)ds.$$

Then, reusing the log-norm $\mu(A)$ [26] as in Theorem 2, we obtain

$$\big\|X(t) - X_p(t)\big\| \leq \int_{t-\tau}^t \big\|e^{A(t-s)}\big\|r\|R_\theta(s)\|\big\|Cw(s) - Cw(s-\tau)\big\|ds$$
$$\leq r\int_{t-\tau}^t e^{\mu(A)(t-s)}\|C\|L\tau\,ds = r\|C\|L\tau\frac{e^{\mu(A)\tau} - 1}{\mu(A)}.$$

Therefore, $\|\Delta X(t)\|_P \leq r\sqrt{\lambda_{max}^P}\|BK\|r\|C\|L\tau\frac{e^{\mu(A)\tau}-1}{\mu(A)} = \beta\gamma$, so that

$$\frac{d}{dt}\|Y(t)\|_P^2 \leq -Y^\top(t)QY(t) + 2\|Y(t)\|_P\big(\|\Delta C(t)\|_P + \|\Delta X(t)\|_P\big) \leq -\frac{\lambda_{min}^Q}{\lambda_{max}^P}\|Y(t)\|_P^2 + 2\beta(1+\gamma)\|Y(t)\|_P.$$

Indeed, $Q \succ 0$ yields $-Y^\top QY \leq -\lambda_{min}^Q Y^\top Y$ [25] and $\|Y\|_P^2 \leq \lambda_{max}^P Y^\top Y$ leads to $-Y^\top Y \leq \frac{-1}{\lambda_{max}^P}\|Y\|_P^2$. Hence, we obtain

$$\frac{d}{dt}\|Y(t)\|_P^2 \leq -2\alpha\|Y(t)\|_P^2 + 2\beta(1+\gamma)\|Y(t)\|_P.$$

Since $\frac{d}{dt}\|Y(t)\|_P^2 = 2\|Y(t)\|_P\frac{d}{dt}\|Y(t)\|_P$, we have $\frac{d}{dt}\|Y(t)\|_P \leq -\alpha\|Y(t)\|_P + \beta(1+\gamma)$ for $Y(t) \neq 0$. Let us define the function $f(v) := -\alpha v + \beta(1+\gamma)$. The solution of the differential equation $\dot{v}(t) = f(v(t))$ with initial condition $v(0) = \|Y(0)\|_P$ is $v(t) = e^{-\alpha t}\big(\|Y(0)\|_P - \frac{\beta}{\alpha}(1+\gamma)\big) + \frac{\beta}{\alpha}(1+\gamma)$. Since $f(v)$ is Lipschitz in v and $\frac{d}{dt}\|Y(t)\|_P \leq f\big(\|Y(t)\|_P\big)$, the Comparison Lemma of [25] states that $\|Y(t)\|_P \leq v(t)$ for all $t \geq 0$. Then,

$$\|Y(t)\|_P \leq e^{-\alpha t}\left(\|Y(0)\|_P - \frac{\beta}{\alpha}(1+\gamma)\right) + \frac{\beta}{\alpha}(1+\gamma) \xrightarrow[t\to\infty]{} \frac{\beta}{\alpha}(1+\gamma).$$

Since this bound on $\|Y(t)\|_P$ is monotonic, we have $\|Y(t)\|_P \leq \max\left(\|Y(0)\|_P, \frac{\beta}{\alpha}(1+\gamma)\right)$. Then,

$$\left\|Bu_\varepsilon(t)\right\| = \left\|R_\theta^{-1}(t)BK\left(X_{\text{ref}}(t) - X_p(t)\right)\right\| \leq \left\|R_\theta^{-1}(t)\right\|\left\|BK\right\|\left(\left\|X_{\text{ref}}(t) - X(t)\right\| + \left\|X(t) - X_p(t)\right\|\right)$$

$$\leq \|BK\|\left(\|Y(t)\| + r\|C\|L\tau\frac{e^{\mu(A)\tau} - 1}{\mu(A)}\right) \leq \|BK\|\frac{\|Y(t)\|_P}{\sqrt{\lambda_{min}^P}} + \gamma\|C\|L\tau \leq \varepsilon,$$

by definition of ε and using $\left\|R_\theta^{-1}(t)\right\| = 1$. Therefore, $Bu_\varepsilon(t) \in \mathbb{B}^2(0, \varepsilon) = \mathcal{P}_\varepsilon$. To sum up, $Bu(t) = Bu_w(t) + Bu_{\text{ref}}(t) + Bu_\varepsilon(t) \in -C\mathcal{W} \oplus \mathcal{P}_{\text{ref}} \oplus \mathcal{P}_\varepsilon \subseteq -C\mathcal{W} \oplus \mathcal{P} \subseteq B\mathcal{U}$ for all $t \geq 0$. Therefore, control law (18) is admissible and the announced tracking tolerance is verified:

$$\left\|X_{\text{ref}}(t) - X(t)\right\| = \|Y(t)\| \leq \frac{\|Y(t)\|_P}{\sqrt{\lambda_{min}^P}} \leq \max\left(\frac{\|Y(0)\|_P}{\sqrt{\lambda_{min}^P}}, \frac{\beta + \beta\gamma}{\alpha\sqrt{\lambda_{min}^P}}\right).$$

$\square$

Theorem 4 provides a controller with trajectory tracking guarantees for the malfunctioning spacecraft (9). The tracking error is dictated by two main terms β and $\beta\gamma$, which respectively bound the prediction errors on the undesirable thrust $\|\Delta C(t)\|_P$ and the state $\|\Delta X(t)\|_P$. The term $\alpha\sqrt{\lambda_{min}^P}$ is just a conversion factor between the P-norm and the Euclidean norm. The term $\|X_{\text{ref}}(0) - X(0)\|_P$ in the definition of ε ensures that the controller is robust to initial state uncertainty as discussed in Section 3.2. The tracking tolerance of Theorem 4 can also be interpreted as a convergence radius for the controller. Indeed, in the proof of Theorem 4 we showed that $\|X_{\text{ref}}(t) - X(t)\|$ must be small enough for $u_\varepsilon(t)$ to be admissible. If $\|X_{\text{ref}}(0) - X(0)\|$ is too large, control law (18) might not be admissible and the convergence of $X(t)$ to $\mathcal{T}_{\text{ref}}$ cannot be guaranteed. The choice of matrices K, P and Q must then be optimized for the controller to be sufficiently robust to initial state uncertainty. A similar but simplified optimization is discussed in Exercise 9.1 of [25].

We will now implement controller (18) embedded with predictor (17) on the malfunctioning spacecraft dynamics (9) to study its performance over the course of the inspection mission and respond to Problem 1.

6   Numerical simulation

In this section we study whether controller (18) can fulfill the mission scenario of Section 2. Recall that the statement of Problem 1 specifies neither the malfunctioning thruster, nor the regularity of the undesirable thrust signal w, nor the value of the actuation delay τ. As discussed above Fig. 6, tracking the reference trajectory of Fig. 2 appears to only be possible if the malfunctioning thruster is no. 4. Therefore, we will only investigate scenarios featuring the loss of control authority over thruster no. 4. In such a case $\rho_{max} > 0$, which enables us to apply Theorem 4 and use controller (18). Then, to address Problem 1 we will simulate a variety of scenarios with different undesirable thrust signals and different actuation delays. We perform all the simulations in MATLAB and all the codes are accessible on github[2].
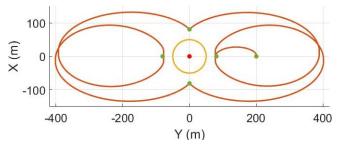

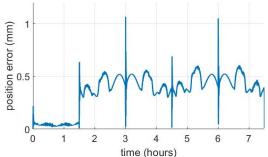[2]`https://github.com/Jean-BaptisteBouvier/Spacecraft-Resilience`

6.1 Nominal scenario

In this first scenario, we choose an actuation delay $\tau = 0.2\,s$ following [16] and a Lipschitz constant $L = 0.1$ for w so that the malfunctioning thrust cannot vary by more than a tenth of its capability every second since $\mathcal{W} = [0, 1]$. We choose matrices K, P and Q to maximize ε subject to $\varepsilon \leq \rho_{max} - \rho_{\text{ref}}$, where $\rho_{\text{ref}} = 4.85 \times 10^{-4}$ is the maximal input norm on the reference trajectory, as seen on Fig. 6. Ample numerical testing on MATLAB led us to believe that the optimal matrices are $Q = I$ and K such that $A - rBK$ has 4 identical eigenvalues. Then,

$$P = \begin{bmatrix} 2.77 & 0 & 1.77 & 0.01 \\ 0 & 2.77 & -0.01 & 1.77 \\ 1.77 & -0.01 & 8 & 0 \\ 0.01 & 1.77 & 0 & 8 \end{bmatrix} \quad \text{and} \quad K = 472 \begin{bmatrix} 1 & 1 & 1 & 1 \\ 1 & -1 & 1 & -1 \\ -1 & -1 & -1 & -1 \\ -1 & 1 & -1 & 1 \end{bmatrix}$$

so that $\varepsilon = 0.4133 < \rho_{max} - \rho_{\text{ref}} = 0.4137$ and the tracking tolerance is $\frac{\beta(1+\gamma)}{\alpha\sqrt{\lambda_{min}^P}} = 1.5 \times 10^{-4}$ for $X(0) = X_{\text{ref}}(0)$.

Then, controller (18) ensures excellent tracking of the reference trajectory $\mathcal{T}_{\text{ref}}$, as shown on Fig. 7(a). We compute the position error between the reference state and the tracking state on Fig. 7(b). We observe that the position error is never larger than $1.07\,mm$ and averages only $0.36\,mm$. We acknowledge that these extremely small errors are only possible because all dynamics, states and thrusts are known exactly in our simple simulation.

(a) Trajectory tracking by controller (18) (red) linking the waypoints (green) to inspect the target satellite (red) without breaching the KOS (yellow).

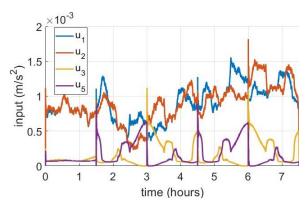(b) Position error between the reference and tracking trajectories.

Figure 7: Analysis of the trajectory tracking performance for a Lipschitz continuous undesirable input w and actuation delay $\tau = 0.2\,s$.

To compare with the tracking tolerance of 1.5×10^{-4}, we also compute the norm difference between the reference and tracking states: $\|X(t) - X_{\text{ref}}(t)\|$. The average norm difference is 3.6×10^{-4}, while the maximal norm difference is 10.5×10^{-4}. Let us investigate why these values are slightly larger than the tracking tolerance. First, note that $\|X(t)\|^2 = x(t)^2 + y(t)^2 + \dot{x}(t)^2 + \dot{y}(t)^2$ where position $(x(t), y(t))$ is of the order of $10^2\,m$ as shown on Fig. 7(a), while velocity $(\dot{x}(t), \dot{y}(t))$ is of the order $10^{-1}\,m \cdot s^{-1}$. Because of these orders of magnitudes, the norm difference between reference and tracking states reflects mostly the position error. Based on Fig. 7(b), the maximal norm difference occurs at 3 hours and 6 hours, i.e., at the waypoints $x = \pm 80\,m$ and $y = 0\,m$ as shown on Fig. 7(a). At every other waypoint Fig. 7(b) also shows error spikes albeit of smaller magnitude. Because the sudden stop and start occurring at each waypoint are not well captured by the discrete dynamics of our simulation, the actual norm difference is larger than the threshold value of Theorem 4.

The undesirable thrust input w is generated as a stochastic signal, whose magnitude is represented in yellow in Fig. 8(a). To counteract w while following the reference trajectory, the controlled input u verifies approximately the intuitive relation $\|u\| \approx \|u_{\text{ref}}\| + \|w\|$. More specifically, Fig. 8(b) shows that thrust inputs u_3 and u_5 replicate the reference thrust profile of Fig. 3b, while u_1 and u_2 counteract malfunctioning thruster no. 4 as expected from their opposite placement on Fig. 1.

(a) Magnitude of the thrust inputs for the reference trajectory $\|u_{\text{ref}}\|$ (blue), for the tracking trajectory the controlled input is $\|u\|$ (red) and the undesirable input is $\|w\|$ (yellow).

(b) Thrust profiles for the four controlled thrusters of the chaser satellite on the tracking trajectory.

Figure 8: Analysis of the thrust profiles of the malfunctioning satellite for a Lipschitz undesirable input w and actuation delay $\tau = 0.2\,s$.

The fuel consumption on the reference and tracking trajectories is displayed on Fig. 9(a). The yellow curve represents the mass of fuel $m_w = 1.06\,kg$ used to produce the undesirable thrust, while the red one shows the mass of fuel $m_u = 1.31\,kg$ used by the controlled thrusters. The reference trajectory without malfunctions requires $m_{\text{ref}} = 0.16\,kg$ of fuel. As expected, $m_u \approx m_{\text{ref}} + m_w$. We have the intuition that the gap between m_u and $m_{\text{ref}} + m_w$ will grow with τ and with the unpredictability of w.

As can be expected from the tracking accuracy displayed on Fig. 7, the velocity tracking of the reference is also extremely accurate with velocities remaining within $0.35\,mm/s$ of each others, as illustrated on Fig. 9(b). As on Fig. 7(b), the error spikes at each waypoint and displays also the same symmetry as the orbit.
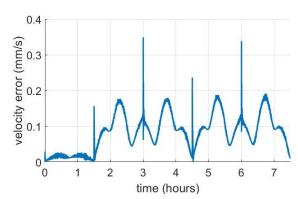
Based on Fig. 7, 8 and 9, controller (18) performs excellently and enables the system to complete its mission when w is Lipschitz continuous and $\tau = 0.2\,s$. To address Problem 1 let us now investigate more challenging scenarios.

6.2   Lipschitz undesirable thrust and actuation delay of 8 seconds

We first increase the actuation delay τ from $0.2\,s$ to $8\,s$ and keep the same Lipschitz and stochastic undesirable thrust signal w. The previous guarantees of Theorem 4 are not valid anymore, but controller (18) still performs sufficiently well to not be distinguishable from the reference as in Fig. 7(a). Instead, we analyze the position error shown on Fig. 10(a). The trajectory tracks the reference with an average position error of $1.2\,mm$ and a maximal error of $4.1\,mm$. These values are extremely low but still represent a fourfold increase compared to the scenario with $\tau = 0.2\,s$.

(a) Comparison of fuel consumption. The mass of fuel used to complete the reference trajectory is m_{ref} (blue). After the loss of control over thruster no. 4, it consumes a mass of fuel m_w (yellow), while the controlled thrusters use a mass m_u (red).
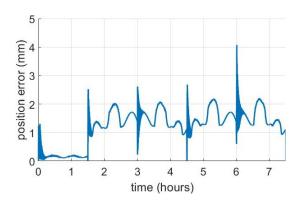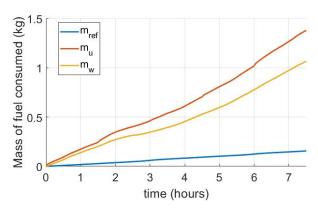
(b) Velocity error between the reference and tracking trajectories.

Figure 9: Comparison of the fuel consumption and velocities for a Lipschitz continuous undesirable input w and actuation delay $\tau = 0.2\,s$.

(a) Position error between the reference and tracking trajectories.

(b) Comparisons of fuel used to complete the reference trajectory m_{ref} (blue), the tracking trajectory m_u (red), and the fuel used by malfunctioning thruster no. 4 m_w (yellow).

Figure 10: Analysis of the trajectory tracking performance for a stochastic Lipschitz undesirable input w and actuation delay $\tau = 8\,s$.

Concerning the fuel efficiency, the pseudo-equality $m \approx m_{\mathrm{ref}} + m_w$ derived from Fig. 9(a) still holds approximately since $m_{\mathrm{ref}} = 0.16\,kg$, $m_w = 1.06\,kg$ and $m_u = 1.38\,kg$ in this scenario. The controlled thrusters have only slightly increased their consumption compared to $m_u = 1.31\,kg$ for $\tau = 0.2\,s$. Thus, the actuation delay does not play as crucial a role for the fuel consumption as for the position error.

6.3 Lipschitz undesirable thrust and actuation delay of 10 seconds

If we increase further the actuation delay, e.g. $\tau = 10\,s$, controller (18) becomes incapable of tracking the reference trajectory as depicted on Fig. 11(a). The velocity on the tracking trajectory is on average four times larger than the reference.

(a) Velocity comparison for the reference trajectory v_{ref} (blue) and the tracking trajectory v (red).

(b) Comparison of input magnitudes with a saturated control $\|u\|$ (red) orders of magnitude larger than the reference $\|u_{\mathrm{ref}}\|$ (blue) and the undesirable input $\|w\|$ (yellow).

Figure 11: Analysis of the trajectory tracking performance for a stochastic Lipschitz undesirable input w and actuation delay $\tau = 10\,s$.

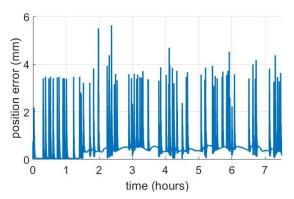The position error has also steeply increased compared to the scenario where $\tau = 8\,s$ since here the average position error is $0.48\,m$ and the maximal error is $3\,m$. These values are still small enough to keep the tracking trajectory indistinguishable from the reference on a figure like Fig. 7(a). However, to maintain this accuracy, controller (18) had to saturate its thrust inputs as shown on Fig. 11(b). This input saturation results in a prohibitive fuel consumption of $503\,kg$ compared to $m_u = 1.38\,kg$ for $\tau = 8\,s$. Now that we have probed the limits of controller (18) in terms of actuation delay, let us investigate the impact of the regularity of w on the tracking performance.
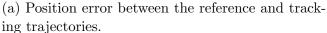
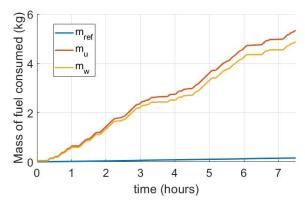## 6.4 Bang-bang undesirable thrust and actuation delay of 1 second

In this scenario we keep the actuation delay $\tau = 1\,s$, but the undesirable thrust signal w is now bang-bang, as illustrated on Fig. 13(a). This violates the Lipschitz assumption of Theorem 4 and hence invalidates its performance guarantees.

Controller (18) generates a trajectory with an average position error of $0.54\,mm$ and a maximal error of $5.6\,mm$ as shown on Fig. 12(a). These values are comparable to the precision achieved in the scenario where w was Lipschitz and $\tau = 8\,s$. As expected, increasing the unpredictability of w from Lipschitz to bang-bang led to a degradation of the tracking performance. Concerning the

fuel usage in this scenario, Fig. 12(b) shows that the bang-bang thrust signal yields a significant consumption increase to $m_w = 4.86\,kg$ compared to $1.06\,kg$ in the Lipschitz scenarios. This increase is reflected on the controller's fuel usage $m_u = 5.33\,kg$, which remains close to $m_{\mathrm{ref}} + m_w = 5.02\,kg$.

(a) Position error between the reference and tracking trajectories.

(b) Comparisons of fuel used to complete the reference trajectory m_{ref} (blue), the tracking trajectory m_u (red), and the fuel used by malfunctioning thruster no. 4 m_w (yellow).

Figure 12: Analysis of the trajectory tracking performance for a bang-bang undesirable thrust signal w and actuation delay $\tau = 1\,s$.

Every time the undesirable thrust climbs to its maximum value, the controller reacts after a delay τ and with a 50% higher spike to makeup for this delay, as illustrated on Fig. 13(a). This overshoot explains the increased mass of fuel consumption by the controlled thrusters. Note also the similarity between Fig. 12(a) and 13(a), each position error spike is associated with a spike of w.
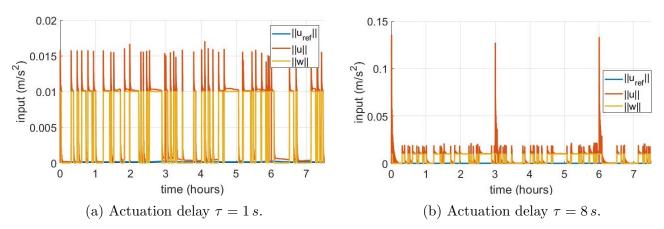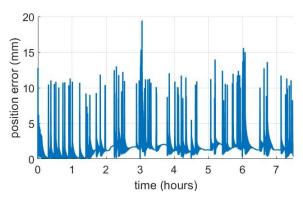

(a) Actuation delay $\tau = 1\,s$.

(b) Actuation delay $\tau = 8\,s$.

Figure 13: Magnitude of the thrust inputs for the reference trajectory $\|u_{\mathrm{ref}}\|$ (blue), the tracking trajectory $\|u\|$ (red), and the bang-bang undesirable input $\|w\|$ (yellow) for different actuation delays.
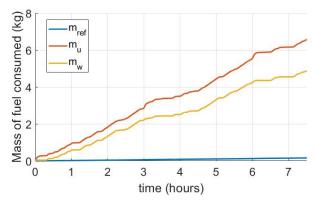
Since controller (18) is still able to track the reference trajectory, we will consider a more challenging scenario with an increased actuation delay.

6.5 Bang-bang undesirable thrust and actuation delay of 8 seconds

We increase the actuation delay to $\tau = 8\,s$ while keeping the same bang-bang undesirable thrust signal as in the previous scenario. The overshoots of the controller have become much larger at three waypoints as shown on Fig. 13(b), while the overshoots at other locations have an amplitude similar to that of w. These large spikes are still an order of magnitude smaller than those of Fig. 11(b), so the controller is not saturating yet.

(a) Position error between the reference and tracking trajectories.

(b) Comparisons of fuel used to complete the reference trajectory m_{ref} (blue), the tracking trajectory m_u (red), and the fuel used by malfunctioning thruster no. 4 m_w (yellow).

Figure 14: Analysis of the trajectory tracking performance for a bang-bang undesirable thrust signal w and actuation delay $\tau = 8\,s$.
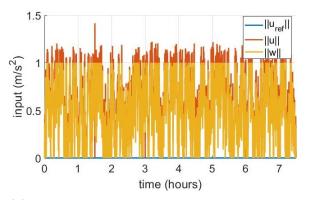
The average position error with respect to the reference trajectory is $1.76\,mm$ and the maximal error is $19.4\,mm$. These values represent approximately a fourfold increase compared to the scenario of Section 6.4. As in the Lipschitz cases where we also witnessed a fourfold increase between $\tau = 0.2\,s$ and $\tau = 8\,s$, the increased actuation delay has significant impact on the tracking accuracy.
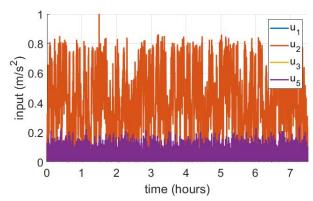
The undesirable thrust still consumes $m_w = 4.86\,kg$ of fuel, but the controller now needs $m_u = 6.56\,kg$ according to Fig. 14(b) instead of $5.33\,kg$ for $\tau = 1\,s$. This consumption increase is most likely caused by the large thrust spikes of Fig. 13(b). As in the Lipschitz case, the increased actuation delay does not have a significant impact on the fuel consumption. However, if we increase τ to $10\,s$, then the situation is similar as that of Section 6.3 with a prohibitive increase in fuel consumption to keep the malfunctioning spacecraft close to the reference orbit.

In all scenarios tested so far, the undesirable thrust signal was saturated at 1% of its capability to have $\|w\|$ of the same order of magnitude as $\|u_{\mathrm{ref}}\|$ as depicted on Fig. 8(a). In the first scenario $\|u\|$ was also of the same order of magnitude. However, we see in this scenario that u sometimes needs to significantly overshoot w. Therefore, we must also investigate the scenario where w has access to its whole thrust capability, i.e., $w(t) \in [0, 1]$, to assess whether it can be counteracted by u despite its saturation limit.

6.6 Saturated Lipschitz undesirable thrust and actuation delay of 2 second

We will now investigate the case of a Lipschitz undesirable thrust input w where $L = 0.1$, $\max\{w(t), t \geq 0\} = 1$ and $\tau = 2\,s$. Since w makes use of its full range of thrust actuation, the controlled thrusters might reach their own saturation limit. The simulation results show the undesirable thrust signal meeting both its saturation limits, $w(t) \in [0, 1]$ as seen on Fig. 15(a). The controlled thrusters however, do not reach their own saturation since the individual magnitude of each thruster never reaches 1 on Fig. 15(b), except at 1 hour 30 minutes. This saturation can also be seen on Fig. 15(a) where $\|u\| = \sqrt{2}$.

(a) Comparison of input magnitude between the reference $\|u_{\mathrm{ref}}\|$ (blue), tracking control $\|u\|$ (red) and the saturated undesirable input $\|w\|$ (yellow).
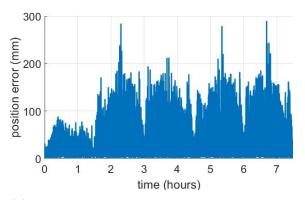
(b) Thrust profiles for the four controlled thrusters of the chaser satellite on the tracking trajectory.
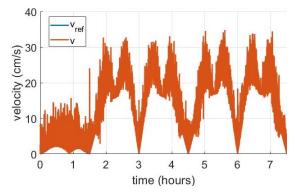
Figure 15: Analysis of the thrust inputs for a Lipschitz undesirable thrust signal w and actuation delay $\tau = 2\,s$.

Based on Fig. 15(b), we can see that thruster no. 2 is producing the thrust necessary to counteract w. Thruster no. 1 is actually matching u_2, just as in Fig. 8(b), except that we cannot see it on Fig. 15(b) because u_2 covers u_1. The average position error is contained to $48\,mm$, while the maximal position error is $0.29\,m$ as shown on Fig. 16(a). Then, the tracking trajectory stays sufficiently close to the reference to not be distinguishable on a figure like Fig. 7(a). The tracking velocity presents large fluctuations above the reference velocity as shown on Fig. 16b(b) while staying much closer than in the scenario of Section 6.3 where v was entirely above v_{ref} as seen on Fig. 11(a).

Because of the large thrusts employed in this scenario, the masses of fuel consumed have also significantly increased. The controlled thrusters would need $m_u = 360\,kg$ of fuel, while the malfunctioning thruster is guzzling $m_w = 342\,kg$ of fuel over the 7.5 hours of the mission. These masses are relatively close, within 5% of each other, which tells us that the controller is not wasting too much extra fuel in overshoots, it uses only what is needed to counteract w. However, recall that our spacecraft mass was set at $600\,kg$. Thus, if such a malfunction were to happen, the thrusters would run out of fuel before completing the mission. Nevertheless, while fuel is available, we now know that controller (18) can compensate time-varying undesirable thrust of maximal amplitude.

With the same Lipschitz undesirable thrust signal, but an actuation delay $\tau = 3\,s$ instead of $2\,s$, the trajectory quickly diverge from the reference. This was somewhat predictable from the saturation of u_2 in Fig. 15(b). Let us now study how controller (18) would fare against a bang-bang undesirable input of similar magnitude.
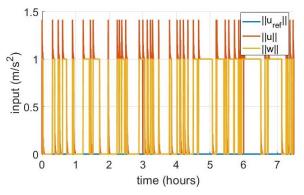
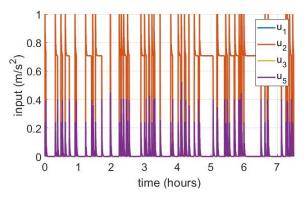(a) Position error between the reference and tracking trajectories.

(b) Velocity comparison for the reference trajectory v_{ref} (blue) and the tracking trajectory v (red).

Figure 16: Analysis of the trajectory tracking performance for a Lipschitz undesirable thrust signal w and actuation delay $\tau = 2\,s$.

6.7 Saturated bang-bang undesirable thrust and actuation delay of 1 second

In this scenario w is bang-bang in $[0, 1]$ and the actuation delay is $\tau = 1\,s$. The simulation shows clearly the bang-bang behavior of the undesirable thrust signal on Fig. 17(a). The controlled thrusters are also reaching their own saturation limit of 1 on Fig. 17(b), except at 1 hour 30 minutes. This saturation can also be seen on Fig. 15(a) where $\|u\| = \sqrt{2}$.
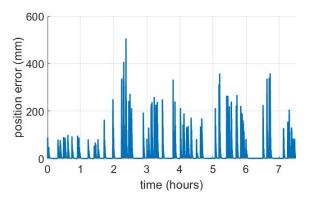

(a) Comparison of input magnitude between the reference $\|u_{\mathrm{ref}}\|$ (blue), tracking control $\|u\|$ (red) and the bang-bang undesirable input $\|w\|$ (yellow).
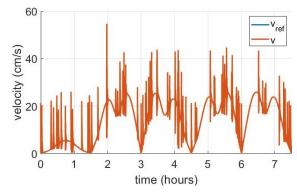

(b) Thrust profiles for the four controlled thrusters of the chaser satellite on the tracking trajectory.

Figure 17: Analysis of the trajectory tracking performance for a bang-bang undesirable thrust signal w and actuation delay $\tau = 1\,s$.

As shown on Fig. 18(a), the average position error is $17.1\,mm$ and the maximal position error is $0.5\,m$, so both trajectories are still indistinguishable on a figure like Fig. 7(a). We note the presence of a velocity spike on Fig. 18(b) for each spike of w on Fig. 17(a).

As in the previous scenario, the fuel consumption is too large for the mission to be completed with such a malfunctioning thruster, but while it is active it can be actively counteracted by u_1 and u_2 as shown on Fig. 17(b). The masses of fuel consumed by u and w are also relatively close, within 3% of each other, with $m_u = 345\,kg$ and $m_w = 336\,kg$, which relates to the efficiency of the controller.

(a) Position error between the reference and tracking trajectories.

(b) Velocity comparison for the reference trajectory v_{ref} (blue) and the tracking trajectory v (red).

Figure 18: Analysis of the trajectory tracking performance for a bang-bang undesirable thrust signal w and actuation delay $\tau = 1\,s$.

If we further increase the actuation delay to $\tau = 2\,s$ for the same undesirable thrust w, the trajectory quickly diverge from the reference. Since the controlled inputs were already saturated for $\tau = 1\,s$ as seen on Fig. 17(b), the controller was not able to overcome a more unpredictable w and this divergence is not surprising.

6.8   Summary of the simulation scenarios

We summarize the scenarios studied above in Table 1. For each scenario, we compute the average and maximal position errors, the mass of fuel used by the controlled thrusters m_u and by malfunctioning thruster no. 4 m_w. We also calculate the relative difference of fuel used $\frac{m_u - m_w - m_{\mathrm{ref}}}{m_w + m_{\mathrm{ref}}}$, which is a good metric for the efficiency of controller (18) in overcoming w without excessive thrust.

Regularity of w	Actuation delay τ	Saturation of w	Average position error	Maximal position error	Fuel used by controlled thrusters m_u	Fuel used by thruster no.4 m_w	Relative difference of fuel used
Lipschitz	$0.2\,s$	0.01	$0.36\,mm$	$1.05\,mm$	$1.31\,kg$	$1.06\,kg$	7.4%
Lipschitz	$8\,s$	0.01	$1.2\,mm$	$4.1\,mm$	$1.38\,kg$	$1.06\,kg$	13.1%
Lipschitz	$10\,s$	0.01	$484\,mm$	$3103\,mm$	$503\,kg$	$1.06\,kg$	41130%
bang-bang	$1\,s$	0.01	$0.54\,mm$	$5.6\,mm$	$5.33\,kg$	$4.86\,kg$	6.2%
bang-bang	$8\,s$	0.01	$1.76\,mm$	$19.4\,mm$	$6.56\,kg$	$4.86\,kg$	31%
Lipschitz	$2\,s$	1	$48\,mm$	$292\,mm$	$360\,kg$	$342\,kg$	5.2%
bang-bang	$1\,s$	1	$17.1\,mm$	$509\,mm$	$345\,kg$	$336\,kg$	2.6%

Table 1: Summary of the simulation scenarios.

Let us now summarize the findings of the various scenarios studied. Despite the narrow range of application of Theorem 4, controller (18) provides tracking accuracy to the millimeter scale on a wide range of scenarios with fast-varying undesirable inputs and long actuation delays. A potential issue limiting the application of controller (18) was the expected saturation of u when w reaches its maximal amplitude. However, scenarios of Section 6.6 and 6.7 showed that for small

actuation delays a maximal w can still be efficiently counteracted. We can visually summarize the performance of controller (18) with the Pareto front of Fig. 19 describing the maximal the saturation limit of w allowing successful tracking at a given actuation delay τ. Based on the scenarios investigated in this section, we decided to consider the tracking to be successful when the position error is always smaller than $0.8\,m$, which is 1% of the minimal target distance on the reference trajectory.
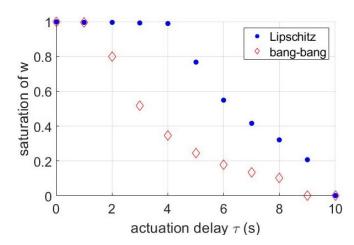

Figure 19: Pareto front of the maximal saturation limit of w for which controller (18) maintains a position error under $0.8\,m$ despite actuation delay τ.

To conclude, after the loss of control authority over thruster no. 4, controller (18) ensures completion of the inspection mission for any undesirable thrust signal w as long as the actuation delay is inferior to $1\,s$.

7   Conclusion and future work

We presented a new methodology to safely perform a satellite inspection mission despite the loss of control authority over a thruster of the inspecting satellite, whose controller is further plagued by a constant actuation delay. To mitigate these issues, we developed resilience theory for linear systems with actuation delay before extending these results to the nonlinear dynamics of the spacecraft under study. We established analytical trajectory tracking guarantees on a resilient feedback controller embedded with a state predictor to compensate for the actuation delay. This controller enables a resilient tracking of the reference trajectory and a safe completion of the inspection mission even when the uncontrolled thruster produces maximal bang-bang inputs.

There are several promising avenues of future work. First, we want to implement our controller on a high-fidelity simulator to study its robustness to unmodeled dynamics. We also have the objective of extending resilience theory to more general nonlinear frameworks, which would enable the study of spacecraft dynamics combining position and attitude for a more realistic treatment.

Acknowledgment

References

[1] C. Aliprantis and K. Border, *Infinite Dimensional Analysis: A Hitchhiker's Guide.* New York: Springer, 2006.

[2] D. C. Woffinden, "On-orbit satellite inspection: navigation and δv analysis," Master's thesis, Massachusetts Institute of Technology, 2004.

[3] N. M. Horri, K. U. Kristiansen, P. Palmer, and M. Roberts, "Relative attitude dynamics and control for a satellite inspection mission," *Acta Astronautica*, vol. 71, pp. 109 – 118, 2012.

[4] J. Diaz and M. Abderrahim, "Visual inspection system for autonomous robotic on-orbit satellite servicing," in *9th ESA Workshop on Advanced Space Technologies for Robotics and Automation*, 2006.

[5] M. A. Vavrina, C. E. Skelton, K. D. DeWeese, B. J. Naasz, D. E. Gaylor, and C. D'souza, "Safe rendezvous trajectory design for the Restore-L mission," in *29th AAS/AIAA Space Flight Mechanics Meeting*, 2019, pp. 3649 – 3668.

[6] J.-B. Bouvier and M. Ornik, "Resilient reachability for linear systems," in *21st IFAC World Congress*, 2020, pp. 4409 – 4414.

[7] M. Bartels, "Russia says 'software failure' caused thruster misfire at space station," *space.com*, 2021, https://www.space.com/space-station-nauka-arrival-thruster-fire-update.

[8] L. Y. Wang and J.-F. Zhang, "Fundamental limitations and differences of robust and adaptive control," in *2001 American Control Conference*, 2001, pp. 4802 – 4807.

[9] D. A. Marsillach, S. Di Cairano, and A. Weiss, "Abort-safe spacecraft rendezvous in case of partial thrust failure," in *59th IEEE Conference on Decision and Control*, 2020, pp. 1490 – 1495.

[10] L. Breger and J. How, "Safe trajectories for autonomous rendezvous of spacecraft," *Journal of Guidance, Control, and Dynamics*, vol. 31, no. 5, pp. 1478 – 1489, 2008.

[11] G. Tao, S. Chen, and S. M. Joshi, "An adaptive actuator failure compensation controller using output feedback," *IEEE Transactions on Automatic Control*, vol. 47, no. 3, pp. 506 – 511, 2002.

[12] B. Xiao, Q. Hu, and P. Shi, "Attitude stabilization of spacecrafts under actuator saturation and partial loss of control effectiveness," *IEEE Transactions on Control Systems Technology*, vol. 21, no. 6, pp. 2251 – 2263, 2013.

[13] A. A. Amin and K. M. Hasan, "A review of fault tolerant control systems: advancements and applications," *Measurement*, vol. 143, pp. 58 – 68, 2019.

[14] J.-B. Bouvier and M. Ornik, "Designing resilient linear systems," *IEEE Transactions on Automatic Control*, vol. 67, no. 9, pp. 4832 – 4837, 2022.

[15] J.-B. Bouvier, K. Xu, and M. Ornik, "Quantitative resilience of linear driftless systems," in *SIAM Conference on Control and its Applications*, 2021, pp. 32 – 39.

[16] R. J. Patton, F. J. Uppal, S. Simani, and B. Polle, "Robust fdi applied to thruster faults of a satellite system," *Control Engineering Practice*, vol. 18, no. 9, pp. 1093 – 1109, 2010.

[17] N. Ortolano, D. K. Geller, and A. Avery, "Autonomous optimal trajectory planning for orbital rendezvous, satellite inspection, and final approach based on convex optimization," *Journal of the Astronautical Sciences*, vol. 68, pp. 444 – 479, 2021.

[18] J.-B. Bouvier, H. Panag, R. Woollands, and M. Ornik, "Resilience of orbital inspections to partial loss of control authority of the chaser satellite," in *2022 AAS/AIAA Astrodynamics Specialist Conference*, 2022.

[19] P. Dumazert, F. Marchandise, L. Jolivet, D. Estublier, and N. Cornu, "PPS-1350-G qualification status," in *40th AIAA/ASME/SAE/ASEE Joint Propulsion Conference and Exhibit*, 2004.

[20] J.-B. Bouvier and M. Ornik, "Quantitative resilience of linear systems," in *20th European Control Conference*, 2022, pp. 485 – 490.

[21] O. Hájek, "Duality for differential games and optimal control," *Mathematical Systems Theory*, vol. 8, no. 1, pp. 1 – 7, 1974.

[22] J.-B. Bouvier and M. Ornik, "Resilience of linear systems to partial loss of control authority," *Automatica*, p. 110985, 2023.

[23] H. Sussmann and V. Jurdjevic, "Controllability of nonlinear systems," *Journal of Differential Equations*, vol. 12, pp. 95 – 116, 1972.

[24] R. F. Brammer, "Controllability in linear autonomous systems with positive controllers," *SIAM Journal on Control*, vol. 10, no. 2, pp. 339 – 353, 1972.

[25] H. K. Khalil, *Nonlinear Systems*. Prentice Hall, 2002.

[26] C. Van Loan, "The sensitivity of the matrix exponential," *SIAM Journal of Numerical Analysis*, vol. 14, no. 6, pp. 971 – 981, 1977.

[27] I. Kolmanovsky and E. G. Gilbert, "Theory and computation of disturbance invariant sets for discrete-time linear systems," *Mathematical Problems in Engineering*, vol. 4, no. 4, pp. 317 – 367, 1998.

[28] V. Léchappé, E. Moulay, F. Plestan, A. Glumineau, and A. Chriette, "New predictive scheme for the control of LTI systems with input delay and unknown disturbances," *Automatica*, vol. 52, pp. 179 – 184, 2015.

[29] R. Kalman and J. Bertram, "Control system analysis and design via the "second method" of Lyapunov: continuous-time systems," *Journal of Basic Engineering*, vol. 82, no. 2, pp. 371 – 393, 1960.

[30] G. H. Golub and C. F. Van Loan, *Matrix Computations*. The Johns Hopkins University Press, 2013.